Fibre volume fractions' and printing directions' effects on tribological and mechanical properties in FDM printed carbon fibre reinforced PEEK

Suitability assessment of FDM printed PEEK-CF to act in a steam engine's ball joint, by analysis of compressive properties, impact strength, friction and wear

Fibervolymers och printningsriktningars påverkan på tribologiska och mekaniska egenskaper i FDM-printad kolfiberförstärkt PEEK

Lämplighetsbedömning av FDM-printad PEEK-CF att verka i en ångmotors kulled, genom analys av kompressiva egenskaper, slagseghet, friktion och nötning

William Tönnberg

Faculty of Health, Science and Technology
Degree Project for Master of Science in Mechanical Engineering
30 ECTS Credits/HP
Supervisors: Pavel Krakhmalev
Examiner: Mikael Grehk
2022-10-06

Abstract

The purpose with this study was to investigate FDM/FFF manufactured carbon fibre reinforced PEEK and assess its suitability to act as a sealing- and bearing material in a modern steam engine's ball joint. The steam engine is totally free from oil due to the risk of water- and steam contamination. Therefore, water-hydrostatic bearings are used in the ball joints which puts high requirements on the sealing- and bearing material's mechanical and tribological properties. PEEK specimens containing 10% and 20% short carbon fibres were printed in a Creatbot F430-3D-printer of FDM/FFF type. Compressive strength and stiffness were investigated in approximately 90 °C for both horizontal and vertical printing layers. Impact strength testing was performed in room temperature with the crack directions crack arrest and crack divider. Tribo-discs were printed, polished and their friction and wear investigated in dry sliding as well as in cold and hot water against a stainless steel sheet of EN 1.4301 (SAE 304/AISI 304), rolled to surface finish 2B.

Compared with injection moulded or FDM printed PEEK-CF with well optimised printing parameters, all specimens had both exceptionally low strengths (26 MPa – 52 MPa), and compressive stiffnesses (0.20 GPa – 0.61 GPa). Most of the compressive specimens exhibited an additional stiffness change long before yielding, which likely were due to layer sliding. It is probable that a higher chamber temperature would result in both better layer- and fibre-matrix adhesion as well as higher crystallinity which would lead to higher strength and stiffness. Horizontally printed PEEK-CF20 had highest stiffness, impact strength and transversal isotropy. PEEK-CF20 exhibited lower friction and wear than PEEK-CF10. Despite that vertically printed PEEK-CF20 was slightly stronger than the horizontally printed, the low degree of transversal isotropy in a vertical design may be inappropriate since it entails a risk for increased water leakage. Hence, horizontally printed PEEK-CF20 is the most suitable material to be used as interfaces and sealings in the steam engine's ball joints.

Sammanfattning

Syftet med denna studie var att undersöka FDM/FFF-tillverkat kolfiberförstärkt PEEK och bedöma dess lämplighet att agera som tätnings- och lagermaterial i en modern ångmotors kulled. Ångmotorn är helt oljefri på grund av risken för kontaminering av vatten och ånga. Därför används vattenhydrostatiska lager i kullederna vilket ställer höga krav på tätnings- och lagermaterialets mekaniska och tribologiska egenskaper. Testningsprover av PEEK innehållande 10% och 20% korta kolfibrer printades i en Creatbot F430-3D-printer av FDM/FFF-typ. Kompressiv styrka och styvhet undersöktes i ungefär 90 °C för både horisontella och vertikala printningslager. Slagseghetstester utfördes i rumstemperatur med sprickriktningarna crack arrest och crack divider. Tribodiskar printades, polerades och deras friktion och nötning undersöktes i torr glidning samt i kallt och hett vatten mot en rostfri plåt av EN 1.4301 (SAE 304/AISI 304), valsad till ytfinish 2B.

Jämfört med formsprutat eller FDM-printat PEEK-CF med väloptimerade printningsparametrar, så hade alla testningsprover både exceptionellt låga styrkor (26 MPa – 52 MPa), och kompressiva styvheter (0.20 GPa – 0.61 GPa). De flesta kompressiva testningsprover uppvisade en ytterligare styvhetsändring långt före plasticering vilket troligtvis berodde på lagerglidning. Det är troligt att högre kammartemperaturer skulle resultera i bättre lager- och fiber-matris-adhesion samt högre kristallinitet vilket skulle leda till högre styrka och styvhet. Horisontellt printad PEEK-CF20 hade högst styvhet, slagseghet och transversell isotropi. PEEK-CF20 uppvisade lägre friktion och nötning än PEEK-CF10. Trots att vertikalt printad PEEK-CF20 var aningen starkare än horisontellt printad så kan den låga graden av transversell isotropi i en vertikal design vara olämplig i kulleden eftersom det innebär risk för ökat vattenläckage. Följaktligen är horisontellt printad PEEK-CF20 det lämpligaste materialet att använda som tätnings- och lagermaterial i ångmotorns kulleder.

Acknowledgements

I would like to thank the following people for supporting me in my master's thesis:

- Pavel Krakhmalev, my supervisor at Karlstad University, for your guidance, support and fast response throughout this period.
- Mikael Fallqvist, my co-supervisor at Karlstad University, for giving me a deeper insight into both your wonderful personality and immeasurable enthusiasm for the exciting world of tribology. Many thanks for your help with the tribological tests and all fruitful and joyful discussions.
- Peter Platell, CEO at RANOTOR AB, for giving me the opportunity to write this thesis and introducing me to your revolutionising steam engine.
- Rasmus Löfstrand Grip, CTO at RANOTOR AB, for all your guidance, support and fruitful discussions. Your effective and illustrative workstyle via digital means of communication never ceased to impress me.
- Henrik Svärd, CEO at Invencon AB, for the opportunity to write this thesis, introducing me to RANOTOR and your hospitality at your office in Karlstad.
- Stefan Mastonstråle & Mohamad Sadek, at Maston AB, for your great and important work with providing me the necessary materials. Your time and help have been unvaluable for the feasibility of this project.
- University personnel Dimitrios Nikas, research engineer, & Mikael Åsberg, university lecturer, for helping me with compressive tests and tribo-tests, respectively.
- Johan Samuelsson & Anders Söderbäck, fellow thesis workers at RANOTOR, for your fruitful discussions and comradeship during the last five years at Karlstad University.

Glossary of terms

PEEK — *Polyether-ether-ketone*

PEEK-CF% — *Carbon fibre reinforced PEEK, (with percentage carbon fibre)*

T_g — *Glass transition temperature*

T_m — *Melting temperature*

AM — *Additive Manufacturing*

FDM — *Fused Deposition Modelling*

FFF — *Fused Filament Fabrication*

CAD — *Computer Aided Design*

COF — *Coefficient of Friction*

FEA / FEM — *Finite Element Analysis/Method*

Table of contents

Table of Figures

Table of tables

1. Introduction

1.1 Company background

The Swedish company RANOTOR is situated in Sigtuna and work with research and development of modern small-scale high-speed steam engines. The background of RANOTOR's steam engine development dates to 1968 when aeroplane and automobile manufacturer Saab was merged with the truck and bus manufacturer Scania-Vabis, formed Saab-Scania and started their steam engine project named RAN [1]. Much money and effort were put into the project, but it came to a halt in 1978 due to new efficient catalytic converters for internal combustion engines (ICE) and large bulky steam engine designs, inter alia [1, 2]. Ove Platell who was the leader of the RAN project at Saab-Scania started his own company in 1983 for further research and development in a modern steam engine. RANOTOR has since then gained much detailed and useful knowledge through both in-house research and via different student projects and theses. The name RANOTOR is a fusion of **Ran**kine and m**otor** since Rankine is the thermodynamical cycle used in steam engines [1].

1.2 Engine applications

The extraction and combustion of fossil fuels, e.g., oil, coal and natural gas, release huge amounts of carbon dioxide, nitrogen oxides and other greenhouse gasses into the atmosphere. The consequential global warming and pollution of health-degenerating particles lead to much greater risks for extreme weather like hurricanes, tsunamis, floods, and drought. It can result in huge mass migration streams, higher sea levels, mass poverty and starvation. Hence, to lower the world's greenhouse gas emissions, is the biggest and most important challenge the human species and its civilisation ever has encountered [3]. RANOTOR's steam engine may be one of many tools to stop or decelerate the climate change. There are many suitable and feasible applications for a reliable and durable modern small-scale steam engine, both stationary and mobile. For example, it can be used in cogeneration plants which is a combined heat and power plant where the waste heat from the electricity generating processes is taken care of as useful heat. Bottoming cycle plants is another feasible application. The main purpose with bottoming cycle plants is to produce high temperature heat to be used in industrial processes. An electricity generating steam engine can be used in bottoming cycles processes combined with waste heat recovery. A mobile application of a small-scale steam engine is to incorporate it into heavy vehicles with internal combustions engines. By letting the hot exhaust gasses from the ICE, heat a steam boiler and use the hot steam in a steam engine, a higher overall fuel efficiency can be reached [2].

1.4 Ball and socket joint

Usage of lubricating oil in the engine would infuse a risk of oil clogging in the small steam pipes due to the high working temperature. For that reason, RANOTOR's aim is to design an oil-free steam engine which results in several difficult tribological challenges. One of these challenges is the contact surface in the ball joint between piston rods and wobble plate. During the spring of 2022, an engineering consultant company named Maston AB, positioned south of Gävle, Sweden, will design and manufacture two steam engine prototypes on behalf of RANOTOR. Their plan is to use 3D-printed carbon fibre reinforced polyether-ether-ketone (PEEK-CF) as interface material in the ball joints. Fused Deposition Modelling (FDM) is the type of 3D-printing technique that will be used for PEEK-CF manufacturing. The engine components that are in direct contact with the super-critical steam will experience temperatures of up to 500 °C. However, the lower parts of the engine where the lower ball joints are located are estimated to have temperatures between around 80 °C and 100 °C. The maximum vertical loads in the ball joints are estimated to be around 96 kN. Due to the extreme loads and absence of oil lubricants, hydrostatic water bearings will be used. A schematic description of the ball joint can be seen in Fig. 1. If the external water pump to the hydrostatic bearings fails or if contact between piston rod and the carbon fibre reinforced PEEK occur for some other reason, a low friction and wear rate is desirable. High impact strength, transversal isotropy and compressive strength and stiffness of the PEEK-CF interface material are also of high importance.

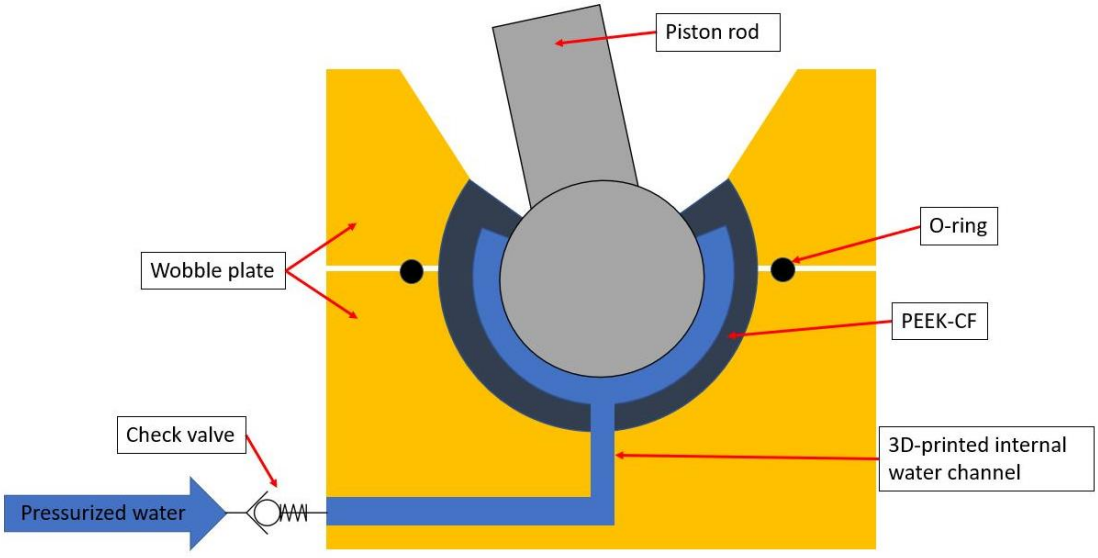

Fig. 1. Schematic description of the ball joint.

1.5 Research questions

- How do different volume fractions of carbon fibre reinforcements influence impact strength, compressive strength and stiffness in 3D-printed PEEK-CF?
- How do different volume fractions of carbon fibre reinforcements influence friction and wear between the PEEK-CF and the counter material in the steam engine's ball joint?
- How do different printing directions influence impact strength, transversal isotropy, compressive strength and stiffness in 3D-printed PEEK-CF?
- Is 3D-printed PEEK-CF a suitable material to be used as interface in the ball joint and what is in that case, the most appropriate printing direction and fibre volume fraction?

2. Theory and literature study

A literature study on FDM-printing of PEEK has been conducted and is presented in this chapter along with interesting and relevant information and theories.

2.1 Engine description

The steam engine from RANOTOR uses super-critical steam at around 250 bar and 450 °C - 500 °C as the working medium and is niched to a power level between 10 kW and 1000 kW. The engine type is an axial piston machine with five cylinders. Each piston is coupled to a stainless steel piston rod which in turn is coupled to a titled wobble plate. In the most common Otto and Diesel engines with crankshafts, the piston rods are linked to the pistons and crankshafts with revolute joints. Due to the rolling and wobbling motion of the wobble plate in the steam engine, the piston rods in the axial piston machine cannot reciprocate in a straight vertical motion. They will instead have an eight-like motion which inhibits the use of revolute joints. Therefore, the piston rods will be coupled to the pistons and wobble plate with ball joints. The high-pressure steam enters the cylinders via a rotating valve (ROV) or some other valve mechanism. This causes large compressive forces in the piston rods which results in rolling of the wobble plate. A vertical Z-shaft is positioned in the centre of the engine and its wobble plate. To create a moment on the Z-shaft and avoid entanglement of the piston rods, some type of synchronization is needed. One possible synchronization type that RANOTOR has investigated is a synchronizing gear mesh. The large vertical compressive forces in the piston rods must be taken up by something. One solution from RANOTOR is to let the wobble plate roll around the Z-shaft on a conical surface. Type sketches of the steam engine during one revolution of the Z-shaft can be seen in Fig. 2. An exploded view with some of the main engine components can be seen in Fig. 3.

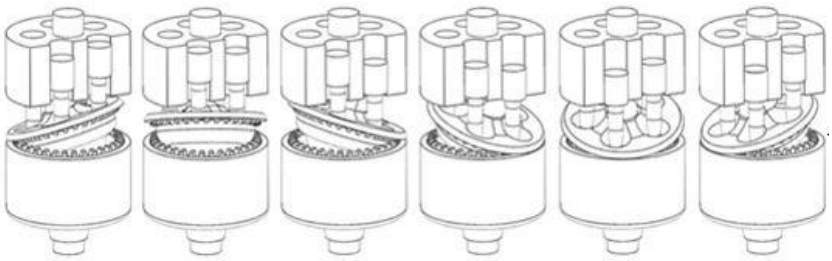

Fig. 2. The steam engine during one Z-shaft revolution [2].

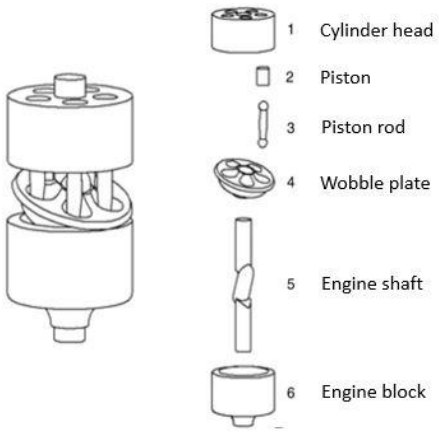

Fig. 3. Exploded view with main components [2].

2.2 Polyether-ether-ketone

Polyether-ether-ketone (PEEK) is an organic semi-crystalline engineering thermoplastic which belongs to the polyaryl-ether-ketone (PAEK) family. Examples of common PAEK-polymers include PEK, PEEK, PEKK, and PEKEKK, where PEEK is the most used. The polymers in the PAEK-family have linear molecular structures of aromatic rings coupled together via different combinations and proportions of ether and ketone groups [4]. An ether group is an oxygen atom bonded to two alkyls or aryls. A ketone group consist of a carbonyl group (carbon atom doubled bonded with oxygen), where the carbon atom is further bonded to two different carbon-containing substituents. In PEEK, two thirds of these groups are ether and one third are ketone. The ether groups contribute to flexibility in the molecule while the ketone groups contribute to rigidity [5]. The chemical structure of the repeating unit in PEEK is shown at the bottom in Fig. 4.

The scientific but rarely used name of PEEK is poly (oxy-1, 4-phenylene-oxy-l, 4-phenylenecarbonyl-l, 4-phenylene) [6]. According to Kurtz et al. [4], there are two main routes to polymerize and produce PEEK: the nucleophilic route and the electrophilic route. The nucleophilic route is the most common, more straight forward and hence will be described in this paper. The nucleophilic process was patented by Imperial Chemicals Industries in 1977 where PEEK has been sold under the brand name “Victrex PEEK” since 1978. PEEK is produced by a step-growth polymerization of 4,4´-difluorobenzophenone and bisphenate in a solvent of diphenyl sulfone [7, 4]. A combination of hydroquinone and potassium carbonate is used to form bisphenate in situ, due to its sensibility to oxidation. The nucleophilic process route for PEEK polymerization can be seen in Fig. 4. Temperatures over 300 °C are necessary to achieve successful polymerisation and high molecular masses. The polymerisation can be terminated and chain length controlled by introducing a small excess of 4,4´-difluorobenzophenone which results in fluorine atoms being bonded to the chain ends. Due to the chemicals involved and the required high temperatures, polymerization of

PEEK is a difficult process that demands tough safety precautions and procedures. For that reason, PEEK is produced in batches instead of continuous processes [4]. As can be seen in Table 1, all these difficulties are reflected in the price. 1 kg of PEEK costs around 545 SEK which is more than 50 times the price of polypropylene.

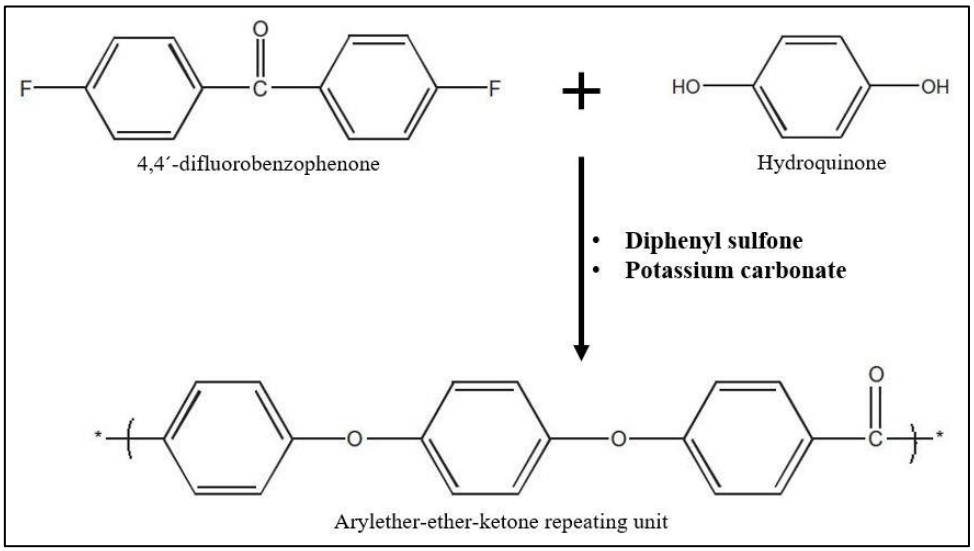

Fig. 4. Nucleophilic process route for PEEK polymerisation.

In relation to the most existing polymers, PEEK has superior stiffness, strength and has a low coefficient of linear thermal expansion. Its thermal and chemical performance is extraordinarily good with a melting temperature T_m of around 343 °C, a glass transition temperature of around 143 °C and a service temperature of around 260 °C [7]. PEEK is very chemically stable and inert since the only organic solvent that can solve it in room temperature is 98% sulfuric acid [4]. PEEK, polyether-ketone-ketone (PEKK), polyetherimide (PEI), Nylon 6 (PA6), and acrylonitrile butadiene styrene (ABS) are often considered as engineering polymers because of their good mechanical, thermal and chemical performance. All of them are thermoplastics and can therefore be used in a FDM 3D-printer. Approximate prices as well as physical and mechanical properties of PEEK and some other thermoplastics commonly used in FDM-printing can be seen in Table 1. As is seen in Table 1, PEEK has the highest yield strength and elongation among the chosen polymers. Only PEKK has higher stiffness (4.4 GPa) than PEEK (3.8 GPa), in accordance with the previous statement that ketone groups provide rigidity. PEKK's greater stiffness comes at the expense of less elongation, in accordance with the ether groups' flexibility. A relatively low density of 1.3 g/cm^3 gives PEEK a high specific stiffness and strength where the specific strength is comparable to and even higher than many steels which makes it an interesting and useful material in many specific high demanding applications. PEEK has radio-transparency and is biocompatible with the human body with a stiffness much closer to the human bones (6-30 GPa) than steel or titanium. It is therefore a remarkably promising material for orthopaedic and dental implants since different

elastic moduli between bones and implants can cause stress shielding and fracture. Much research is currently being made on carbon fibre reinforced PEEK for implant purposes since carbon fibre reinforced PEEK exhibits higher strength and perfect elastic modulus in the range of human bones [8].

Table 1. Approximate properties of PEEK and some other polymers, for comparison purposes only [9].

Material	**Young's modulus [GPa]**	**Density** $[\frac{g}{cm^3}]$	**Yield strength (room temp.) [MPa]**	**Elongation at break [%]**	**Glass transition temp.** T_g **[°C]**	**Melting temp.** T_m **[°C]**	**Price** $[\frac{SEK}{kg}]$
Polyether-ether-ketone (PEEK)	3.8	1.3	90 - 110	30-150	143 - 157	322 - 346	545
Polyether-ketone-ketone (PEKK)	4.4	1.3	70-110	11-13	153-170	347-373	815
Polyetherimide (PEI)	3.0	1.3	74 - 81	55-65	216	354 - 394	155
Polylactic acid (PLA)	3.5	1.3	55	10-20	52 - 60	145 - 175	25
Nylon 6 (PA6)	0.9 – 1.2	1.1	39 - 48	40-60	44 -56	210 - 220	25
Acrylonitrile butadiene styrene (ABS)	2.4	1.1	40	5-60	88 - 120	210 - 250	15
Polypropylene (PP)	1.5	0.9	35	50-230	-14 – (-6)	161 - 170	10

2.2.1 Water absorption

It is well-established knowledge that most polymers absorb water in humid environments which can result in changes of physical and mechanical properties. At room temperature and above, water is a sort of plasticizer since it can be seen as spacers between the polymer chains. Water absorption often result in decreased elastic modulus, strength, and glass transition temperature but increased elongation and impact strength. However, only water molecules linked to the polymer chains via hydrogen bonds affect the polymer's properties. Since the ketone groups in PEEK are strongly dipolar and can form hydrogen bonds with absorbed water molecules, it may be suspected that PEEK is sensitive to water absorption [10]. However, PEEK is relatively resistant against water. One study showed that PEEK exhibited only a 5% decrease in tensile strength after it had been laid in 100 °C water for 322 days [11]. Wang et al. [12] tested water absorption in injection moulded PEEK and PEEK-CF30 after 24 h in 23 °C water. PEEK-CF30 absorbed much less water than pure PEEK, 0.06% and 0.5%, respectively [12]. As a rough comparison, nylon-6 and nylon-6,6 has water absorption saturation values of about 9.5% and 8%, respectively. Water absorption and diffusion in a polymer is very much dependent on the available free volume. Therefore, the water diffusion

occurs mainly in the amorphous sections in semi-crystalline polymers. Consequently, polymers with higher degrees of crystallinity generally have less water absorption [13]. Lay et al. [14] analysed water absorption in FDM-printed specimens of PLA, ABS and nylon-6 compared to injection moulded ones. It was found that FDM-printed PLA, ABS and nylon-6 had 133%, 102% and 89% more water absorption compared to their injection moulded reference specimens, respectively [14].

2.2.2 Crystallinity

As previously mentioned, PEEK is a semi-crystalline polymer which means it contains both amorphous and crystalline regions. The amorphous regions have a very low or non-existent degree of molecular conformational order while the crystalline regions exhibit a high degree of long-range order. In fact, no polymers are fully crystalline since they are either amorphous or semi-crystalline. When a polymer is heated over the glass transition temperature T_g, the molecules in the amorphous sections can make discrete jumps. A consequence of the allowed discrete jumps is a sudden drop of elastic modulus of the order of 10^3 [15]. An increase of crystallinity is often desirable since it can result in higher strength, stiffness, and working temperatures but at the expense of decreased toughness and ductility [16]. When a semi-crystalline thermoplastic is cooled from a melt, short sections of some of the previously randomly folded molecular chains assumes their lowest energy-state [15]. In PEEK, it means that the chains straighten up with a zig-zag backbone. The straight sections of the chains are then packed next to one another, and form ordered crystals with orthorhombic crystal structures [11, 15]. Random local ordering of molecules as well as different kind of impurities, including carbon fibre can act as nucleation sites for crystal growth in PEEK. The crystals are spheres in the very beginning of the crystallisation process but eventually grow to form so called spherulites which can be described as flat discs with alternating amorphous and crystalline lamellas in the hoop direction. Spherulites grow until they are either impinged by other neighbouring spherulites or impurities such as carbon fibres [11]. A study by Chen et al. [17] investigated crystallisation and spherulitic growth in PEEK and PEEK-CF. The study showed that carbon fibres impinged growing spherulites and decreased crystallisation rate, leading to smaller spherulites and less degree of crystallinity. McCrum et al. [15] means that, in similarity with grain crystallisation processes in metals, solidification at low temperatures results in small spherulites due to high nucleation rate while high-temperature solidification results in large spherulites due to low nucleation rate. An approximation of the temperature for maximum crystallisation growth for many polymers can be acquired by Eq. 2.1, [15].

$$T = 0.8T_m \quad [K] \tag{2.1}$$

Eq. 2.1 with a melting temperature for PEEK of around 343 °C [7], suggest an approximate temperature for maximum crystallisation growth of around 220 °C. In addition to temperature, the degree of crystallinity is greatly influenced by cooling rates where slower cooling rates result in higher crystallinity [11]. The typical degree of crystallinity in PEEK is around 35% [16].

2.3 Additive Manufacturing

Additive Layer Manufacturing (ALM) or simply Additive Manufacturing (AM) is a manufacturing method where three-dimensional (3D) components are created by adding small amounts of material layer by layer. Therefore, these additive manufacturing methods are commonly known under the general name 3D-printing. These techniques differ significantly from the traditional manufacturing methods such as lathing, milling and drilling where the components are formed by subtraction of material from initially larger objects. The usage of AM methods has increased considerably in the last decade and years, mainly because of its ability to allow very complex geometries that cannot be created with the traditional manufacturing methods [18]. AM can have economic benefits since material waste and manufacturing lead times can be significantly reduced [19]. According to Rinaldi et al. [18], lighter and more energy efficient components can be manufactured, hence it is very likely that the usage of AM will increase even more in the future and be a more efficient and environmentally friendly manufacturing method.

2.3.1 Fused Deposition modelling

Regarding polymers and their composites, there are five main different AM techniques available: Laminated Object Manufacturing (LOM), Fused Deposition Modelling (FDM), Multi-Jet Fusion (MJF), stereolithography (SLA) and Selective Laser Sintering (SLS) [19]. According to Dua et al. [5], PEEK can only be 3D-printed by two methods, SLS and FDM. In SLS, fine powder of the chosen material is evenly distributed on a building platform in a thin layer by a roller. A laser beam is directed towards the powder bed in a pre-programmed pattern to fuse the material together. The process is repeated until the whole structure is completed. The SLS process is illustrated in Fig. 5a. SLS printers can achieve resolutions down to 50-100 µm and FDM printers down to 100-150 µm. Despite the better resolutions in SLS, the FDM technique is cheaper and is for that reason commonly the most preferred choice [5]. Solid filaments in FDM are much easier and safer to handle for the workers compared to the fine polymer powder in SLS which can be mistakenly inhaled if managed improperly. There is also less risk for degradation and contamination in filaments than in powder [6].

FDM is the same thing as Fused Filament Fabrication (FFF) and the reason for two existing names is that FDM is an owned trademark. Although FFF is the general and non-trademarked name, FDM

may be the most common term to be used. FDM is a very versatile AM method for 3D-printing of polymers and is in many cases the most preferred method for polymer 3D-printing due to its non-complex technique and low costs. The feedstock materials for FDM printing are in the form of long filaments spun on spools. The filament diameter is usually between 1.75 mm to 2.85 mm. The filament is pulled from the spools by some type of dragging mechanism, usually in form of rollers. Hence, the filament is in tension before the rollers and in compression after them. Thereafter, the filament is pushed toward a heating chamber which converts it to a plastic melt. With the compressive stresses induced by the rollers, the plastic melt can be extruded through a nozzle onto a preheated building platform. The nozzle moves in the xy-plane and extrudes the polymeric strings in a predetermined pattern. Once a layer is finished, the building platforms moves downward in the z-direction allowing a new layer to be printed. The z-distance moved by the platform is the layer height. Smaller layer heights result in finer layers and surface roughness at the expense of longer production cycle times [19]. A schematic illustration of FDM printing can be seen in Fig. 5b.

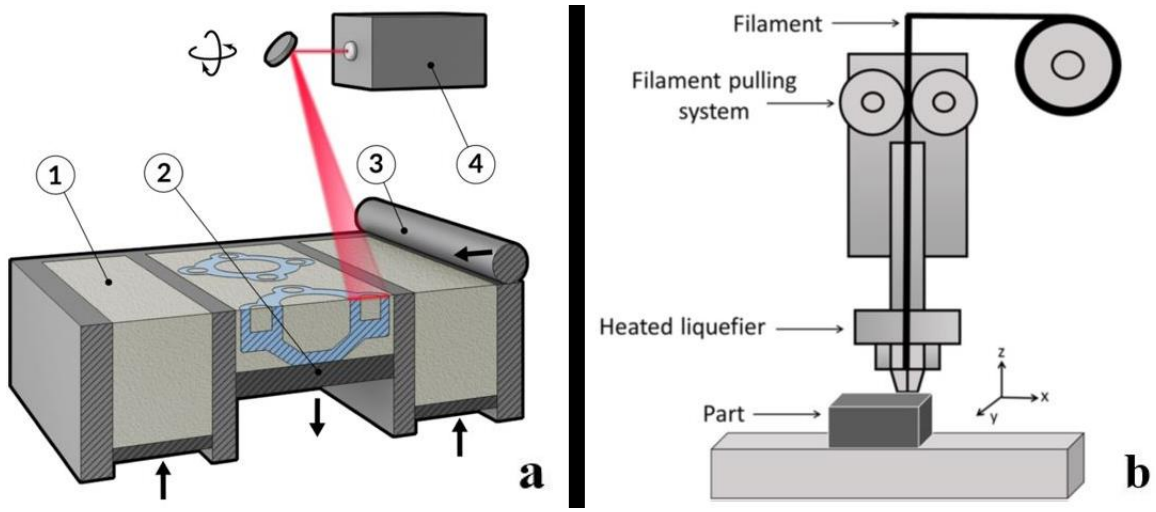

Fig. 5. Schematic pictures of: a) Selective Laser Sintering [20], b) Filament Deposition Modelling [19]. Point 1: Movable powder storage. Point 2: Movable and heated building platform. Point 3: Roller. Point 4: Laser.

Fibre implementation in thermoplastic polymers has displayed significant improvements in mechanical properties such as strength and elastic modulus [21]. Adding of fibres can also reduce bending and warping during the printing process [19, 21]. In AM, usage of short and discontinuous fibres is often preferred due to the complexity and cost of long continuous fibres in these processes. The most common way of fibre implementation in FDM is to mix polymers and fibres and extrude fibre/polymers filaments which is ready to use in a FDM machine [19].

The manufacturing process with FDM printing begins with creating a digital model with Computer Aided Design (CAD). The CAD-model is converted to and stored as a STL-file where the surface

geometry is represented by many triangles. The more triangles, the better approximation of the real model geometry. Thereafter. The STL-file is put into a slicer-program which translates all the necessary printing parameters such as extruder nozzle movements, temperatures, and layer heights into a so-called G-code [19].

2.3.2 FDM printing parameters

Achieving adequate mechanical and physical properties of 3D-printed polymers is quite challenging due to the unavoidable anisotropic-resulting layer-by-layer technique [7]. Engineering thermoplastics such as PEEK, PEI and PA with high melting temperatures and glass transition temperatures are the most difficult to 3D-print. Despite the significant increase of FDM-usage the last decade and years, there are only a few FDM printers that are capable of printing these engineering polymers due the high temperatures needed to melt them [18]. There are several important parameters that in a high or low degree affect physical and mechanical properties of a finished FDM printed object.

Infill density: The infill density describes the ratio between the predetermined extruded volume and the whole volume of the component. In harmony with the intuition, higher infill densities result in better mechanical properties, such as modulus and strength. Infill density shall not be confused with the relative density or packing density which is the ratio between the actual printed volume and the intended printed volume. Those volumes are never the same due to undesired air pores arising in the printing process [22].

Nozzle diameter & layer height: Common nozzle diameters for PEEK printing is 0.4 mm and above. Wang et al. [23] investigated mechanical performance for pure PEEK specimens, FDM-printed with different nozzle diameters, layer heights and nozzle temperatures. It could be concluded that the 0.4 mm nozzle resulted in relatively little change of tensile strength and density when layer height, printing speed and nozzle temperature were varied. Usage of the 0.6 mm and 0.8 mm nozzles led to more unstable processes when the other parameters were varied. Generally, the 0.4 mm nozzle resulted in the highest tensile strength, density, and lowest surface roughness, regardless of the other printing parameters. When polymer is extruded, the nozzle gently pushes down on the printing layers and smear out the strings to achieve better compaction. Consequently, the layer height is lower than the nozzle diameter. Increased layer height always results in worse surface roughness. In Wang's et al. [23] study, layer height had low impact on tensile strength when a 0.4 mm nozzle was used. However, the tests with 0.6 mm and 0.8 mm nozzle diameters resulted in decreased strength, layer adhesion, and density with increased layer height and remarkably poor mechanical performance obtained with layer heights exceeding 0.35 mm. The surface roughness increased significantly when the layer height exceeded 0.5 times the nozzle diameter. Wang's study

also concluded that maximum tensile strength was obtained with layer heights approximately equal to half the nozzle diameter. Highest tensile strengths for 0.4 mm, 0.6 mm, and 0.8 mm of nozzle diameter were obtained with layer thicknesses of 0.25, 0.3, and 0.35, respectively [23].

Nozzle temperature: The nozzle temperature may be one of the printing parameters that affect the properties of the finished objects the most. Wang et al. [21] conducted a study where tensile, flexural and impact strengths' dependence of nozzle temperatures in pure PEEK and PEEK-CF5 were investigated. Temperature ranges tested were from 400 °C to 440 °C in intervals of 10 °C. The study showed that increased nozzle temperatures resulted in higher strengths due to better material fluidity and interlayer adhesion. SEM analyses showed a significantly better wrapping of the PEEK matrix around the short carbon fibres for specimens printed at 440 °C. According to Zanjanijam et al. [7], nozzle temperatures influence the polymer crystallisation process where higher temperatures lead to higher crystallinity and consequently higher tensile strengths and moduli. Finding a suitable and optimised nozzle temperature is crucial to achieve good mechanical properties. A too low temperature can lead to material clogging in the nozzle and weak interlayer adhesion. A too high nozzle temperature can cause thermal degradation of the polymer matrix. Lower surface roughness can be achieved with higher nozzle temperatures due to better fluidity and higher diffusion of polymer macromolecules [7]. Ding et al. [22] investigated how the nozzle temperature affected the relative density in FDM printed pure PEEK. Ding's study tested nozzle temperatures up to 420 °C and found that increasing nozzle temperatures resulted in increased relative densities which reached values of 92.8%. The obtained relationship is due to better material fluidity at higher temperatures.

Chamber temperature: Many FFF/FDM machines have heated printing chambers since the ambient temperature has significant impact on dimensional accuracy and mechanical performance. Large temperature differences between nozzle and chamber causes rapid cooling which can result in warpage distortion and internal stresses [7]. As already outlined in section 2.1.2, rapid cooling reduces the degree of crystallinity. Crystalline sections exhibit lower toughness and ductility compared to amorphous sections, but higher stiffness and strength due to larger intermolecular forces in the densely packed molecular chains. A study by Yang et al. [16] investigated chamber temperature's effect on crystallinity and mechanical properties in FDM-printed PEEK. The chamber temperature was varied between 25 °C and 200 °C. The study showed that 200 °C resulted in highest crystallinity, elastic modulus, and tensile strength, at the expense of lower breaking elongation [16]. Some manufacturers of PEEK 3D-printers have recently explored the possibility to use lower chamber temperatures resulting in a rapid cooling but with subsequent annealing. The lower chamber temperature and fast cooling result in an amorphous component but with less shrinkage and better stress distribution. Thereafter, the component is annealed to allow chain movement and crystallisation [7].

Platform temperature: Only a few studies have investigated the platform temperatures effect on the properties of the finished printed parts. Even less have investigated the effects with PEEK and its composites. A high adhesion friction between the first printed layers and the platform is important to achieve a good result. There is an impendent risk for warping and delamination if the adhesion friction is insufficient. But if the adhesion is too high, the part can be damaged during cooling [24]. According to Zanjanijam et al. [7], higher platform temperatures enhance adhesion to platform, material diffusion, bonding, and surface roughness, though nozzle temperature has a greater impact on surface roughness than platform temperature. In Wang's et al. [21] study with pure PEEK and PEEK-CF5, it was concluded that higher platform temperatures led to enhanced tensile, flexural and impact strengths, less interlayer gaps and better interlayer bonding, presumably due to increased material fluidity and diffusion. Spoerk et al. [24] investigated platform temperatures' effect on the adhesion between platform and printed objects in PLA and ABS. The study showed that the adhesion increased steadily up to the glass transition temperature. A very large increase in adhesion forces takes place slightly above the T_g due to enhanced polymer chain mobility and diffusion to the platform-polymer interface. Additional temperature increases lead to lower adhesion. Maximum adhesion is expected to occur slightly above T_g with other thermoplastics as well, such as PEEK. When printing larger parts, the warpage can be substantial which counteracts the adhesion force. Therefore, the adhesion friction must be higher for larger parts than smaller parts. It is desirable to have a frictional force of at least 200 N when printing larger parts [24].

Raster angle: The raster angle describes in which directions the printing strings are laid in the xy-plane. For example, a raster angle of ±45° in a rectangular component means that the printing strings will vary 90° between two different layers while the strings will have an angle of 45° relative the component's straight sides. According to Yang et al. [16], the macromolecular polymer chains are often strongly oriented in the strings along the printing direction in FDM due to its unidirectional melt-extrusion process through the small nozzle. Therefore, the printing stings are stronger and stiffer in the longitudinal direction than the transverse direction. Consequently, unidirectionally FDM-printed PEEK specimens can exhibit higher longitudinally elastic moduli than injection moulded ones. However, FDM-printed specimens rarely have higher tensile strength due to defects and pores from the 3D-printing process.

Heat treatments: Post printing heat treatments can significantly improve crystallinity and mechanical properties. Yang et al. [16] investigated how different heat treatments affect crystallinity and mechanical performance in FDM-printed pure PEEK. The studied heat treatments were air cooling, furnace cooling, quenching, annealing, and tempering. All specimens were printed with a chamber temperature of 100 °C. The annealing was executed in 200 °C with no allowed

cooling between printing and heat treatment. The tempering process consisted of an initial air cooling with a sequential tempering in 250 °C. Annealing resulted in the highest crystallinity of 38%, followed by furnace cooling and tempering with 36% and 34%, respectively. Air cooling and quenching resulted in low crystallinities of 30% and 28%. The different heat treatments' values of stiffness and strengths were consistent with the mutual order of their degree of crystallinity, except for furnace cooling. Specimens with furnace cooling exhibited elastic moduli and tensile strengths significantly lower than the tempered ones. Considering the poor breaking elongation for tempered specimens, Yang et al. [16] concluded annealing and furnace cooling as appropriate heat treatment methods for many applications.

2.4 Fracture toughness and internal interfaces

Because of AM's layer-by-layer technique, AM-manufactured components often contain internal interfaces, voids and other imperfections. Such imperfections may act as crack initiation sites. Depending on crack direction and degree of adhesion, internal interfaces may enhance or reduce fracture toughness. When describing material cracks, the direction of coordinate axes can be chosen arbitrarily. However, the most common way is to let the x-axis be in the crack growth direction and the z-axis parallel to the crack front. Such a coordinate system containing both a crack tip in the origin and a material element with stresses is shown in Fig. 6.

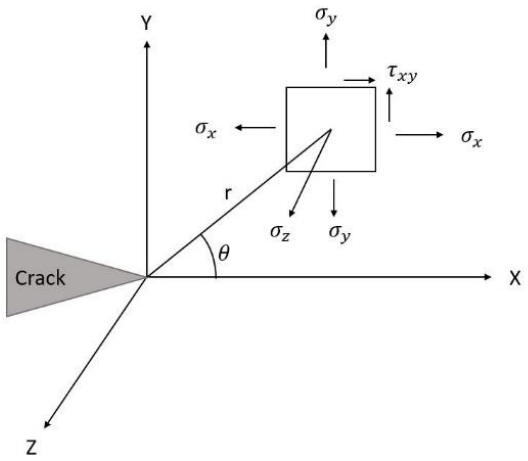

Fig. 6. Stresses on a small element close to a crack tip [25].

According to Hertzberg et al. [25], the stresses on an element in the vicinity of a crack tip can be described with Eq. 2.2 - 2.4. Which can be seen in Fig. 6, r is the distance between crack tip and element while θ is the angle between x- and y-axis.

$$\sigma_y = \frac{K}{\sqrt{2\pi r}} \cos\left(\frac{\theta}{2}\right)\left[1 + \sin\left(\frac{\theta}{2}\right)\sin\left(\frac{3\theta}{2}\right)\right] \quad (2.2)$$

$$\sigma_x = \frac{K}{\sqrt{2\pi r}} \cos\left(\frac{\theta}{2}\right)\left[1 - \sin\left(\frac{\theta}{2}\right)\sin\left(\frac{3\theta}{2}\right)\right] \quad (2.3)$$

$$\tau_{xy} = \frac{K}{\sqrt{2\pi r}}\left[\sin\left(\frac{\theta}{2}\right)\cos\left(\frac{\theta}{2}\right)\cos\left(\frac{3\theta}{2}\right)\right] \quad (2.4)$$

K is the stress intensity factor which describes the magnitude of the stress field in the crack tip. This factor shall not be confused with the stress concentration factor k_t which is the ratio between maximum stress and nominal stress. The stress concentration factor k_t only takes geometric dimensions into consideration while the stress intensity factor K considers both crack length, component shape and how the load is applied. If the stress intensity factor K in a certain component is larger than the materials fracture toughness K_C, the crack will propagate, and failure occur. By analysing the expression for the stresses in Eq. 2.2 - 2.4, the stresses could rise to infinity in the crack tip when the radius is close to zero. However, in reality those extreme rises of stresses are suppressed by plastic deformation at the crack tip [25].

Depending on the thickness and yield strength of the component, two types of stress-strain conditions can occur at a crack front. Since no stress can act normal to a free surface, a thin component in the z-direction would not be able to develop a stress in the z-direction. In these scenarios, only biaxial σ_x and σ_y stresses are present which is why this condition is called plane-stress. In thicker components, σ_z stresses can develop and counteract the otherwise negative ε_z strain. In these scenarios, only biaxial ε_x and ε_y strains are present which is why this condition is called plane-strain. For an isotropic material, the strain in the z-direction is described with Eq. 2.5, [25].

$$\varepsilon_z = \frac{1}{E}\left(\sigma_z - \nu\sigma_x - \nu\sigma_y\right) \quad (2.5)$$

If $\varepsilon_z \approx 0$ in Eq. 2.5, the maximum stresses that can develop in the z-direction are $\sigma_z = \upsilon(\sigma_x + \sigma_y)$.

By calculating the effective stress with the stress expressions in Eq. 2.2 - 2.4 while considering load redistribution at the crack tip and the increased effective crack length due to the plastic zone, Irwin obtained estimates of the plastic zone size. Irwin showed that the size of the plastic zone around a crack tip is approximately three times larger in plane stress than in plane strain. The fracture toughness of a material is much dependent on the volume capable to plastically deform. Hence, the

fracture toughness in plane stress is superior to plane strain. Fracture-mode transitions between plane-stress and plane-strain and their generally associated differences in fracture toughness can often be analysed by naked-eye observations of fracture surfaces. High-energy absorbing plane-stress fractures are more likely to have slant fractures rather than flat ones which are more common for plane-strain fractures [25].

In sections 2.3.2 and 2.6 of this report, it is mentioned that the adhesion between layers in FDM-printed PEEK could be relatively weak. Therefore, the layers can be seen as so-called free surfaces. Since no stress can act normal to a free surface, plane stress conditions could be achieved in FDM-printed PEEK components. According to Hertzberg et al. [25], three different types of crack growth situations can develop in such a laminate depending on how the crack is oriented. If the crack is oriented in such a way that its crack front meets the weak interface, $\sigma_x \approx 0$ and plane stress will occur. Even further improvements on fracture toughness can be achieved if layer delamination occur since it will contribute to blunting of the crack tip. This situation is called crack arrest and is illustrated in Fig. 7a. Another crack growth situation can occur if the crack front is normal to the interfaces. In that case, $\sigma_z \approx 0$ and plane stress will occur. That is named crack divider and is illustrated in Fig. 7c. The third possible crack orientation is where the crack goes in between the weak interfaces and cleaves the specimen. This situation is called short transverse and is illustrated in Fig. 7b. Generally, crack arrest and crack divider have superior fracture toughness to short transverse [25].

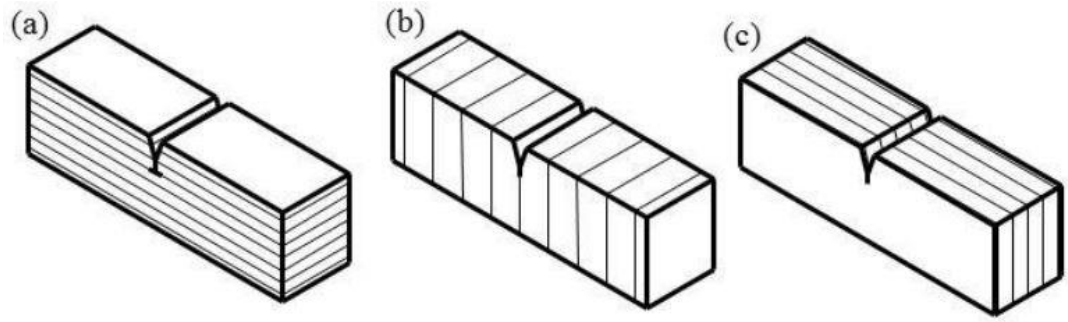

Fig. 7. Specimens with weak internal interfaces: a) Crack arrest, b) Short transverse, c) Crack divider [26].

2.5 Tribology

Tribology involves the study of friction, wear and lubrication in a tribosystem with two or more surfaces in relative motion. It is an old knowledge but relatively new as a scientific discipline and the term “tribology” was first mentioned in 1966 [27, 28]. Friction and wear are no material parameters but a result of a very complex tribosystem dependent on many factors such as environment, surface topography, chemical compositions, stiffness, hardness and ductility.

Tribology is commonly studied with practical experiments due to the great complexity and many influencing parameters [28]. Development in the tribological research area can result in great winnings regarding everything from quality and performance of products to savings of raw materials, environment, energy and economy. For example, it has been estimated that 10% of the oil consumption in the US is related to decreasing friction [29].

Polymers, both plastics and elastomers, have many tribologically dependent properties that differ significantly from metals and ceramics. Elastomers are commonly used in applications demanding high friction and damping while thermosets and thermoplastics can be used in bearings since they often have low friction, wear, weight and price with high corrosion resistance and good formability. The great elasticity contributes to easier achievement of elastohydrodynamic lubrication and makes them almost irreplaceable as sealing materials. Tribological disadvantages of polymers include among other things, low heat conductivity and heat resistance and sensibility to fatigue and high point loads. The tribological properties can be significantly improved by implementation of friction-reducing filler materials such as graphite, MoS_2 and PTFE and strength- and stiffness-improving fibre reinforcements such as glass- and carbon fibres. However, lower ductility as a result of fibre reinforcements can lead to increased wear because less energy is then required to break away a particle [29]. Reinforcement of heat conductive carbon fibres or metal particles can reduce friction heat and minimise the risk for thermal softening or degradation [30].

2.5.1 Friction

For two surfaces in contact, only a small fraction of the apparent area is a true load bearing area. The real area consists of elastically and/or plastically deformed surface asperities. Whether they are elastically or plastically deformed is governed by the asperities' radii of curvature but mostly of the ratio H/E^* where H is the hardness and E^* the reduced modulus. An implicit expression for reduced modulus in a contact between two materials with Young's moduli E and Poisson's ratios ν is given in Eq. (2.6). The hardness can often be approximated as three times the yield strength. Large radii of curvature and possibility to large elastic deformation before plasticity, i.e., high ratio of H/E^*, increases probability to purely elastic contact. A precise limit for when H/E^* would result in plastic or elastic asperity contact cannot be constructed since it is dependent on surface topography. However, metals usually have reduced moduli around 0.01 while it often lies around 0.1 for most polymers and ceramics. It entails that the most surface contacts are plastic for metals but elastic for ceramics and polymers. Only very finely polished metal surfaces can experience predominantly elastic contacts [27].

$$\frac{1}{E^*} = \frac{(1-\nu_1^2)}{E_1} + \frac{(1-\nu_2^2)}{E_2} \tag{2.6}$$

In 1699, Guillaume Amontons stated that the friction force is proportional to the normal load and independent of the apparent area. The statements were based on empirical observations and are relatively accurate for most materials and conditions, with the exception of polymers [27]. The coefficient of friction (COF), which is the ratio between tangential friction force and normal load, is for polymers dependent on load, apparent area, and surface topography and much more sensitive to sliding velocity and temperature compared to metals and ceramics. Polymers' deviations from Amontons' laws are mostly due to their elastic asperity contacts and the real area often being a large fraction of the apparent area. The COF between polymer-polymer or polymer-metal is often in the range 0.1 – 0.5, [29].

Friction has two origins: an adhesive component and a deformation component. The adhesive component is caused by adhesive bonding of the surfaces' contacting real areas. Consequently, the adhesion is proportional to the real area and very dependent on the surfaces' chemical environment. Polar polymers with high fractions of hydrogen bonds generally exhibit larger adhesion than non-polar ones. At low normal loads and rough surfaces, the friction for polymers is proportional to the load. At higher loads or smoother surfaces, the real area transforms into one single contact zone instead of many small ones. The real area then becomes proportional to the load to the power of 2/3 instead of 1, resulting in decreased COF at increased loads. For metals, the adhesive component is usually much larger than the theoretical value because of junction growth and work hardening. Excessive junction growth in metals can cause extreme COFs up to 10 and immediate severe surface failure but is often avoided because of limited material ductility and present low shear strength surface films. However, junction growth is very limited for polymers despite their high ductility [27].

For metals and ceramics, the deformation component originates from the resulting deformation force when asperities in the harder material plough through the softer material. For those cases, the deformation component is more commonly referred to as the ploughing component and is very dependent on surface topography. For polymers however, the deformation component generally is not due to ploughing but friction losses between sliding polymer chains in the bulk material and is therefore less dependent on surface topography [27].

2.5.2 Wear

Wear in polymers is often due to three main wear mechanisms: interfacial wear, cohesive wear, and erosive wear by impacting particles. The interfacial wear occurs at the top surface and originates from adhesive van der Waals or hydrogen bond induced forces between contacting asperities. In most polymers, the interfacial bonds are stronger than the bulk polymer resulting in shear fractures

of asperities. Amorphous polymers, however, tend to have weaker interfacial junctions than the bulk, resulting in minimum adhesive wear [27].

The other mechanism, cohesive wear, is a result of plastic or elastic deformation in a larger area on and beneath the surface of the softer material when it slides against a counterface's harder protuberance or asperity. Repetitive elastic deformations result in micro fatigue and propagation of microcracks while the plastic deformations result in abrasive wear and micro cutting. Abrasive wear can also cause wear by brittle fracture and microcracking, but it is less common in polymers. Soft polymers against smooth counterfaces are more commonly subjected to micro fatigue while abrasion is more likely to occur in stiff polymers with rough counterfaces. The wear in polymers is very dependent of the counterfaces' roughness where smooth counterfaces promote interfacial wear and rough one's cohesive wear. Due to the high ratio of H/E* in polymers, the counterface must have an average roughness (Ra) greater than a few µm to create plastic abrasive wear. The harder particle or asperity must typically be around 1.2 times harder than the softer material to effectively abrade it [27]. A distinction is often made by two-body abrasion and three-body abrasion where the former often results in 10 times more wear [29].

2.5.3 Tribofilm formation

Tribological contacts usually involve high flash temperatures and mechanical strains which increase chemical reaction speeds and introduce new reaction routes. These tribochemical processes and the not totally unavoidable wear, can create tribofilms between the surfaces which can both increase or decrease friction and wear. Tribofilms are often divided into two categories: "Transformation type tribofilms" and "Deposition type tribofilms". Transformation type tribofilms are created by diffusional and chemical processes, phase transformations or plastic deformations. Deposition type tribofilms are formed by material transfer from anywhere in the tribosystem [28, 29].

At sliding of polymer against metal, a thin friction- and wear reducing deposition tribofilm may be formed, consisting of worn polymer chains. A closed tribo-environment and good adhesion to the metal counterface entail very low wear since further wear of the bulk polymer is heavily limited as long the polymer-transfer film is present. The counterface cannot be too rough or too smooth for the polymer-film to adhere properly. A correct amount of abrasive fibre- or particle reinforcement may therefore clean and polish the counterface to an adequate roughness [27]. A deposition tribofilm between a polymer and steel is often immediately destroyed if liquid water is added. It is thought to be due to the so called "hydraulic effect", where water, because of the contact pressure, is squeezed in and out through small pits and pores on the polymer's surface [31].

2.6 Previous studies on PEEK and PEEK-CF

2.6.1 Compressive strength

Rahman et al. [6] investigated how the compressive strength of FDM-printed pure PEEK was affected by different raster angle combinations. The tests were done in accordance with ASTM 695 with building orientation parallel to compression direction. Two different raster angle combinations were studied: 0° and alternating layers of 0°/90°. The mean compressive yield strength for 0° was around 66 MPa while the mean value for 0°/90° was around 54 MPa. The higher strengths for the single raster specimens were likely due to the smaller stress bearing area, especially since a relatively low nozzle temperature of 340 °C and a very high nozzle diameter of 1.8 mm was used [6]. Another study by Han et al. [32] studied the compressive strength for FDM-printed pure PEEK and PEEK-CF5. The standard was ISO 604 but the tested building direction and raster angle are not presented. Han found that the compressive strengths for both pure PEEK and PEEK-CF5 were statistically the same at around 138 MPa which is about the same as injection moulded PEEK, (≈140 MPa), [8, 33], which was not the result Rahman's et al. [6] study. Compared to Rahman, Han used better printing parameters with for example a nozzle temperature of 420° and a nozzle diameter of 0.4 mm [32].

Carbon fibre fractions' effect on compressive strength in injection moulded PEEK was studied by Qin et al. [8]. Specimen with 0%, 25%, 30%, 35% and 40% carbon fibres were tested according to ISO 604:2002 standard and resulted in roughly 140 MPa, 190 MPa, 190 MPa, 185 MPa and 215 MPa, respectively. The explanation for a decline in strength for 30% and 35% was aggregation of carbon fibre bundles which act as stress concentrations. With fractions over 25%, poor polymer wrapping around the fibres was revealed which resulted in fibre pull-out rather than fibre fracture in the flexural strength tests that also was conducted in the study. However, the fibre reinforcing effect began to dominate with 40% carbon fibre [8]. Another study by Li et al. [33] studied the compressive strength for injection moulded pure PEEK, PEEK-CF25 with short fibres (150-200 µm) and PEEK-CF25 with long fibres (2-3 mm). The testing standard was ISO 604:2002 and the compressive strengths were 137 MPa, 196 MPa and 450 MPa, respectively. The significantly higher compressive strengths for the long fibred specimens compared to the short fibred were due to more uniform stress distribution along the long fibres [33]. The previous studies of compressive strength with short fibres are presented in this section are compiled in a graph in Fig. 8.

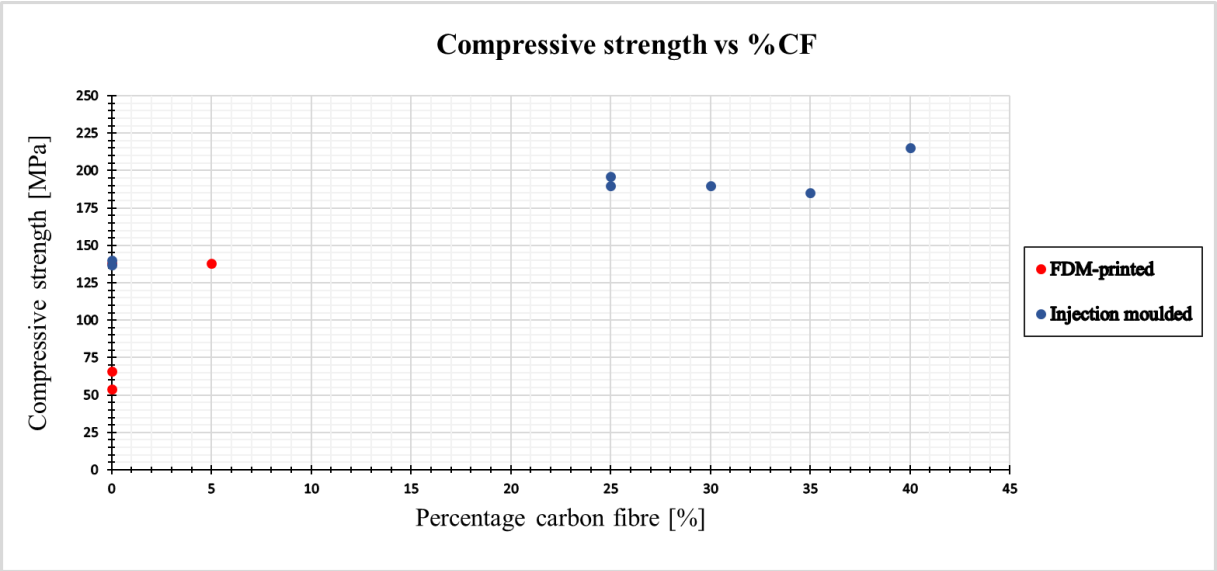

Fig. 8. Compressive strength as a function of percentage carbon fibre.

2.6.2 Impact strength

Wang et al. [21] investigated how the impact strengths of FDM-printed PEEK and PEEK-CF5 were affected by nozzle temperature, platform temperature and printing speed. Charpy impact testing was done in accordance with ISO-179-1:2010. The specimens were unnotched, printed with alternating raster angles of ±45° and tested in the crack arrest direction with a flatwise impact. The study showed that the pure PEEK had roughly twice the impact strength as PEEK-CF5, independent of the various printing settings. The nozzle temperature had a relatively low influence on the impact strength, although the highest nozzle temperature of 440 °C resulted in best impact performance. The authors believed that the worse impact strength in PEEK-CF5 was because of pores arising in the PEEK-carbon fibre mixing in the filament manufacturing [21].

Another study by Ding et al [22] investigated nozzle temperatures effect on impact strength for FDM-printed pure PEEK. The specimens had dimensions in conjunction with ISO 179-1:2010. Notched Charpy-V specimens with raster angles of ±45° were tested in crack arrest and crack divider directions. In contrary to the results obtained by Wang et al. [21], the tests by Ding showed that both low and high nozzle temperatures led to worse impact strengths. The best impact strength was obtained with a medium nozzle temperature of 390 °C. This indicates that the best interlaminar bonding doesn't necessarily result in the highest impact strength. This interesting phenomenon may come from the fact that the layer interfaces are too strong and therefore cannot be seen as weak interfaces. Recall from section 2.3 that weak interfaces may allow a transition from plane strain to the more favourable plane stress situation. Crack arrest had significantly higher impact strength than crack divider at all nozzle temperatures except at the highest at 410 °C and 420 °C where crack divider showed marginally better impact strength. Crack divider experienced layer spallation which

lowers the impact strength. Ding also conducted the same tests for PEI. Noteworthy from Ding's tests is that the impact strength for PEI was almost independent of both nozzle temperature and crack direction due to only brittle fractures while the PEEK specimens experienced both brittle and ductile fractures [22].

Rahman et al. [6] investigated how the impact strength of FDM-printed pure PEEK was affected by different raster angle combinations. Charpy-V impact testing was done in accordance with ASTM 6110 which has slightly different specimen dimensions than ISO 179-1:2010. Pure PEEK was tested in crack arrest with 3 raster angle combinations: 0°, 90° and alternating 0°/90° where the 0° direction was parallel to the specimens' long sides. The study showed that raster angles of 0° had significantly better impact performance than the others. Raster angles of purely 90° had slightly higher impact strength than alternating 0°/90°, which the authors believe depend on the poor interlaminate bonding with alternating layers [6]. As already mentioned in the previous section, Rahman used relatively poor printing parameters.

A study by Qin et al. [8] examined the impact strength for injection moulded PEEK with different fractions of short carbon fibres. Testing was executed according to ISO 179-1:2000 with unnotched Charpy specimens containing 0%, 25%, 30%, 35% and 40% carbon fibres. The study showed that an increase of hardness and decrease in impact strength occur for higher carbon fibre fractions. An interesting result was that the impact strength decreased significantly from 35% to 40% carbon fibre, which may indicate an upper suitable limit. Graphs with impact strength and hardness for the different fibre fractions can be seen in Fig. 9, [8].

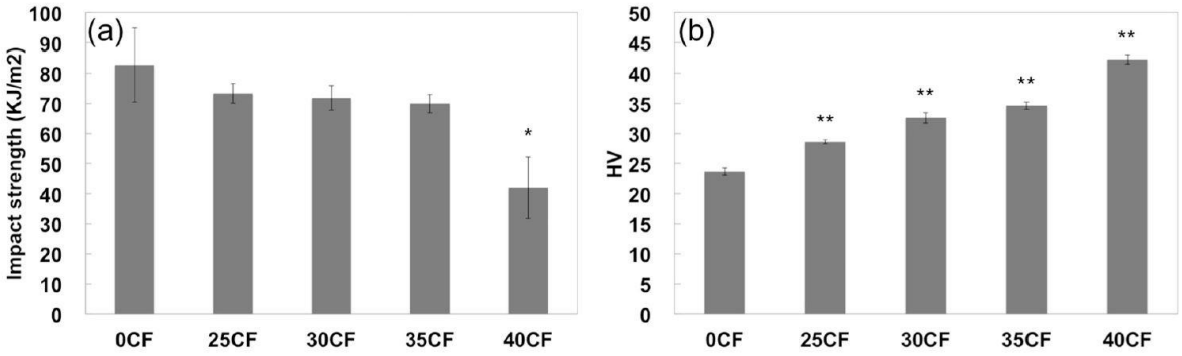

Fig. 9. Impact strength and hardness for PEEK and PEEK-CF [8].

2.6.3 Friction and wear

Jacobs et al. [30] investigated friction and wear for inter alia, injection moulded pure PEEK, PEEK-CF30 and glass fibre reinforced PEEK (PEEK-GF40) against (AISI 304 = EN 1.4301 stainless steel), martensitic bearing steel EN 1.3505 and aluminium oxide Al_2O_3. Testing was conducted in both dry condition and in deionised water with average contact pressures between 3 and 17 MPa. The friction and wear of PEEK-CF are much dependent of its ability to create a smooth and dense lubricating transfer film of fine graphite particles from decomposed worn carbon fibres. Pure PEEK without carbon fibres cannot create such a film and its friction and wear is therefore less dependent on counter material, though often having more wear in water due to moisture absorption. The tribology for PEEK-CF is more complicated. In water, PEEK-CF could not create a lubricating transfer film against any of the tested counter materials. Alumina was the only counter material where friction was lower in water since it cannot form a lubricating transfer film in dry conditions due to its chemical inertness. Harder counter materials often lead to less wear of polymers. This is clearly the case with alumina which resulted in low friction and wear, where the major influencing factor was surface roughness. Except for chemically inert ceramics, wear of PEEK and PEEK-CF is higher in water. Possible explanations for that are combinations of moisture absorption, no transfer film formations and tribocorrosion with consequential three body abrasive wear of loose rust particles [30].

PEEK-CF30 against AISI 304 in dry conditions first resulted in a gradual increase of friction up to a sliding distance of around 80 m when the value of COF suddenly dropped to 1/3 to μ=0.17 with a wear of 15×10^{-8} mm^3/ (Nm). In water, no beneficial tribofilm was formed and the wear increased significantly to 350×10^{-8} mm^3/ (Nm), despite the water lubrication's friction reduction to μ=0.15. Giltrow et al. [34] tested friction and wear of carbon fibre reinforced thermosetting polymers against different materials. They found that a smooth lubricating transfer film could be formed easier on counter surfaces harder than around 1000HV or on Chromium-rich materials, such as stainless steels. In Jacob's et al [30] study, PEEK-CF30 against the low-Chromium martensitic bearing steel with 850 HV could not form a transfer film resulting in high wear due to tribocorrosion and three body abrasive wear of rust particles. Sliding of PEEK-GF40 in water resulted in very high wear due to the glass fibres sensibility to stress corrosion cracking (SCC). It performed even worse than pure PEEK and reached specific wear values of $4{,}000 \times 10^{-8}$ mm^3/ (Nm) against AISI 304 and $7{,}000 \times 10^{-8}$ mm^3/ (Nm) against Al_2O_3.

3. Materials and methods

3.1 Materials

With the obtained knowledge from previous studies on FDM-printed PEEK and its carbon composites in remembrance, four different materials were selected for further manufacturing and mechanical and tribological testing: pure PEEK and PEEK with 10%, 20% and 30% carbon fibre reinforcement. The materials were procured in the form of filament spools with 1.75 mm in diameter. The pure PEEK, PEEK-CF10 and PEEK-CF20 were supplied by 3DXTECH and consist of Victrex® PEEK. The PEEK-CF30 filaments was supplied by Ensinger and is made of VESTAKEEP® PEEK. Questions regarding fibre length, diameter and whether the carbon fibres are PAN-based or Pitch-based, and have been pre-treated in any way, have been sent to the suppliers. Unfortunately, it could not be revealed due to proprietaries and trade secrets. Tradenames and approximate mechanical and physical properties, according to the suppliers, are given in Table 2. However, it shall be noted that the mechanical properties are highly dependent on printing parameters.

Table 2. Approximate properties of filament materials, according to manufacturers.

Material	Young's modulus [GPa]	Tensile strength [MPa]	Impact strength $[kJ/m^2]$	T_g [°C]
ThermaX PEEK	3.7	100	No data	143
CarbonX PEEK-CF10	8.1	105	No data	143
Carbon X PEEK-CF20	10.1	126	No data	143
TECAFIL PEEK-CF30	19.4	204	55 (ISO 179-1/1eU)	143

The filament manufacturers recommended printing parameters can be seen in Table A1 in Appendix A. All specimens in this project were printed by Maston AB in their Creatbot F430 FDM-printer. All printers on the market have different designs which infuses a need for optimisation of printing parameters. Therefore, initial printing experiments were carried out to find suitable parameters. The printing parameters were optimised through trial and error using the literature study in this report, manufacturers recommended parameters and Maston's previous experience and knowledge as a base. Many difficulties were encountered during the initial printing attempts, mostly involving low platform adhesion and excessive warping. Those problems were solved for PEEK-CF10 and PEEK-CF20 by raising nozzle temperature to 420 °C and spray adhesive glue onto the glass ceramic platform. Because of the adhesive glue, lower platform temperatures than suggested in this report's literature study were used, (see section 2.3.2). Unfortunately, the printing problems for pure PEEK and PEEK-CF30 could not be solved which may be due to the Creatbot F430's limitations. Its maximum nozzle temperature, chamber temperature and platform temperature are 420 °C, 70 °C

and 140 °C, respectively. Due to the limited time frame of this project, only PEEK-CF10 and PEEK-CF20 were analysed. All specimens were annealed according to Fig. 10.

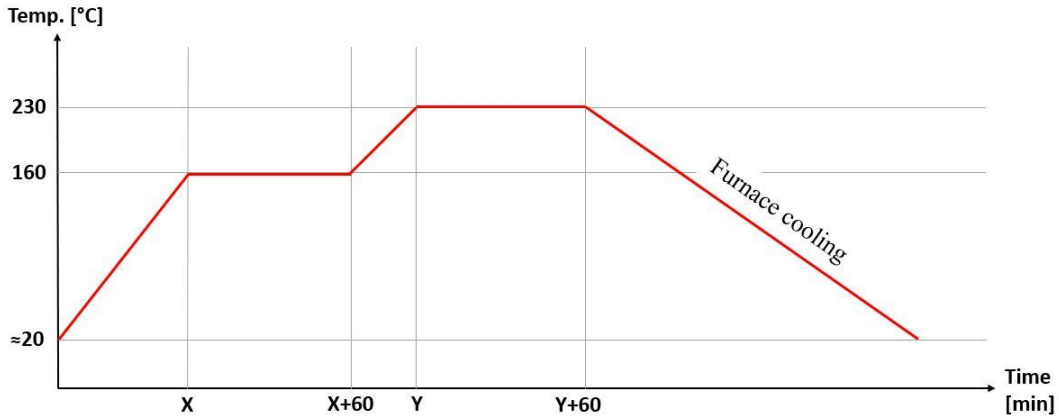

Fig. 10. Annealing process for all specimens and materials.

3.2 Compressive test

The compressive strength of PEEK-CF10 and PEEK-CF20 were tested based on the ISO 604:2002 standard with a servo-hydraulic INSTRON 8501 testing machine. Six specimens were tested for each material type, three with horizontal layers and three with vertical layers. The specimen had raster angles of ±45°, dimensions 10 mm × 10 mm × 4 mm and were printed with one shell layer. The compressive tests were executed in a furnace at around 90 °C at a compression speed of 1 mm/min. In compressive tests for polymers, it is common that the early part of the stress-strain curve is slightly bent due to inter alia slant surfaces or large asperity interactions associated with low surface roughness. Therefore, the specimens were preloaded with 0.5 kN which equals a stress of 5 MPa. A thermocouple was placed around the specimens for temperature control. The crushed specimens were investigated in a stereo microscope. The two specimen types and their approximate slicing setup are shown in Fig. 11. A rigged specimen and the testing machine can be seen in Fig. 12.

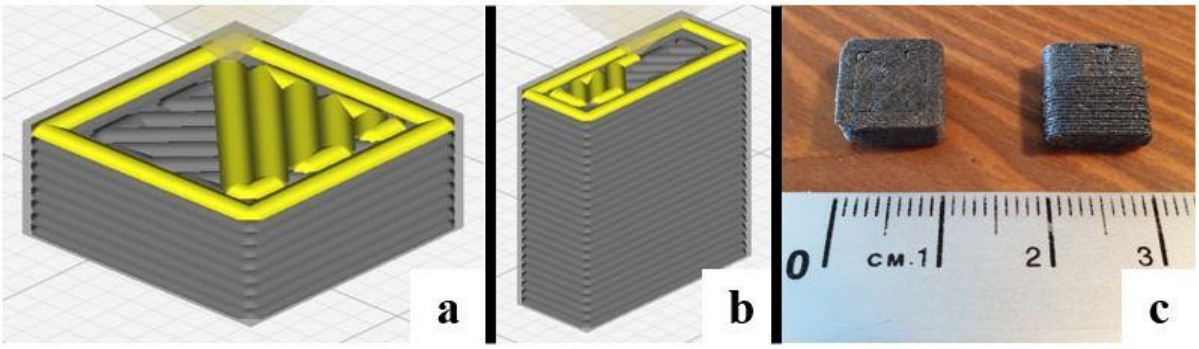

Fig. 11. Approximate slicing setup for compressive specimens for: a) Horizontal layers, b) Vertical layers. c) Compressive specimens, horizontal at the left and vertical to the right.

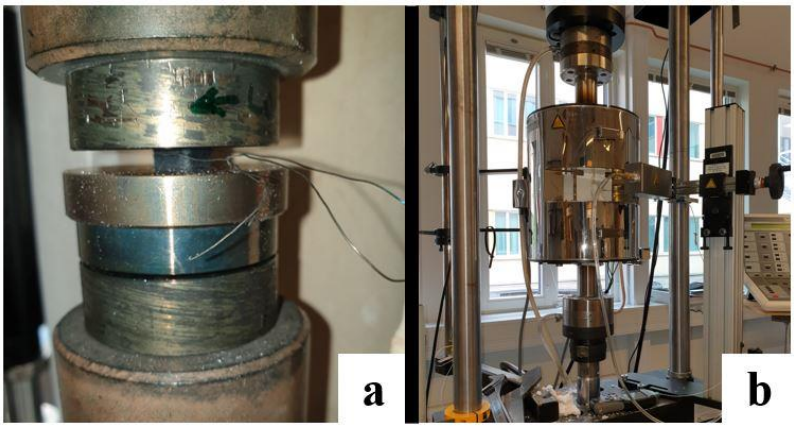

Fig. 12. a) Clamped specimen with thermocouple, b) Servo-hydraulic tester with furnace.

3.3 Impact test

Unnotched Charpy impact strength of PEEK-CF10 and PEEK-CF20 were tested based on the ISO 179-1:2010 standard with a Charpy pendulum. The most interesting crack direction to investigate would have been short transfer since it usually is the weakest. However, FDM-printing of specimens with short transverse requires either support material or an interlink of the specimens that can be broken after printing. This was not feasible due to time limitations, hence only crack arrest and crack divider were tested. Six specimens were tested for each material type, three with crack arrest and three with crack divider. The specimens had raster angles of ±45°, dimensions 80 mm × 10 mm × 4 mm and were printed with one shell layer. The compressive tests were executed with edgewise impact at room temperature with method designation ISO 179-1/1eU. The specimens' fracture surfaces were investigated in a stereo microscope. The two specimen types and their approximate slicing setup are shown in Fig. 13.

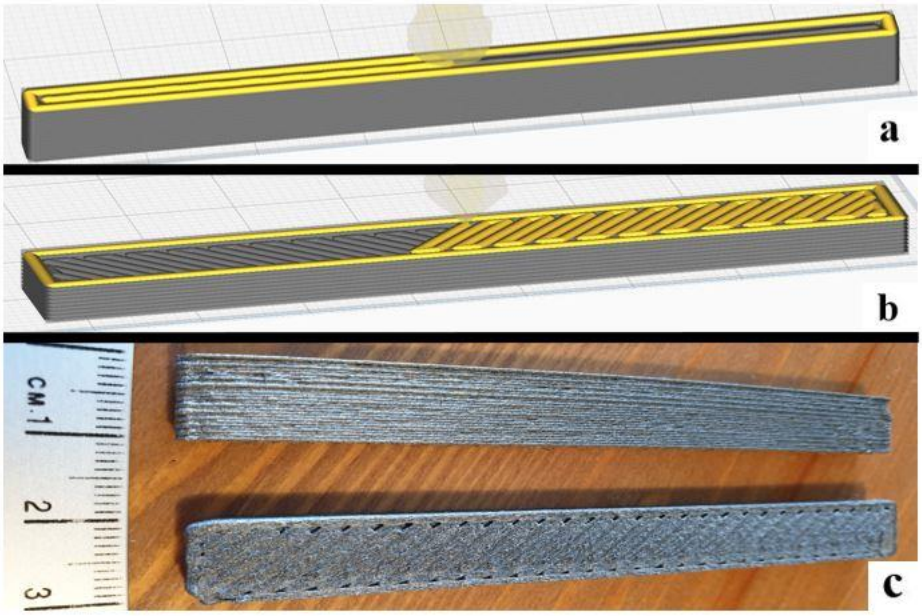

Fig. 13. Approximate slicing setup for impact specimens for: a) Crack arrest, b) Crack divider. c) Impact specimens, crack arrest at the top and crack divider at the bottom.

3.4 Friction and wear

The friction and wear of the different materials were analysed by sliding 3D-printed discs against a stainless steel sheet in Karlstad university's Slider On Flat Surface (SOFS) tribotester. It would be favourably to achieve roughly the same ratios of maximum contact pressures between the different material types in the SOFS-tests as in the supposed real application. Heinrich Hertz presented his well-known theories about analyses of stress fields, deformations, contact pressures, and contact areas in 1881, which commonly is referred to as Hertzian contact mechanics. The aforementioned quantities can be calculated with assumptions of frictionless contacts between two non-conforming, homogenous, isotropic, and linearly elastic materials where the contact area is small compared to the bodies' sizes and radii of curvature [27, 29]. Due to the ball joint's high degree of surface conformity and thin interface section, the Hertzian contact theory is not valid. Therefore, finite element (FE) simulations were performed on the ball joint. FE simulations of all materials, including pure PEEK and PEEK-CF30 were performed since the results may be useful in future works.

3.4.1 FE simulations of ball joint

FE simulations were done with the Finite Element Method (FEM) software ABAQUS. The lower half of the ball joint was modelled with 3D-deformable axisymmetric shell elements. The dimensions are the same as in the steam engine's early prototype. The stainless steel ball has a 15 mm radius. The inner radius of the PEEK/PEEK-CF interface is 15.25 mm, allowing a 0.25 mm

hydrostatic water film. Outer radius of the interface is 16.45 mm resulting in a 1.2 mm interface thickness. Inner radius of the stainless steel socket was also 16.45 mm and its thickness was given an arbitrary and adequate value of 8.8 mm to remove the effects of its encastred outer surface and achieve a more accurate simulation of the joint. The joint was simulated assuming frictionless contact between interface material and ball/socket. The stainless steel material was assigned a Youngs's modulus of 190 GPa and Poisson's ratio ν=0.25. The PEEK/PEEK-CF interface materials were assigned Young's moduli according to Table 2 and ν=0.4. For simplicity, no consideration was taken to eventual material failure or plasticity. The parts were meshed with quad-dominated elements and a convergence study can be seen in Fig. A3 in Appendix A. To achieve better accuracy, the mesh size decreased gradually towards the ball joint's bottom centre where the approximate element size was 0.05 mm.

The FE model consists of three parts: ball, interface and socket and are positioned relative to one another according to Fig. 14. Reference points 1 and 2 are placed at point 1 and point 2. Point 1 is coupled with surface 5 and point 2 is coupled with surface 1. Degree Of Freedom constraints are applied to these points so that surface 5 is encastred while surface 1 is allowed to move only in the Y-direction. Surfaces 2, 3 and 4 are constrained to move in the X-direction. The vertical load is applied on point 2 in the negative Y-direction. This setup allows the interface material to slightly slide upwards when the ball pushes down on it which is clearly seen happening in Fig. A2 in Appendix A.

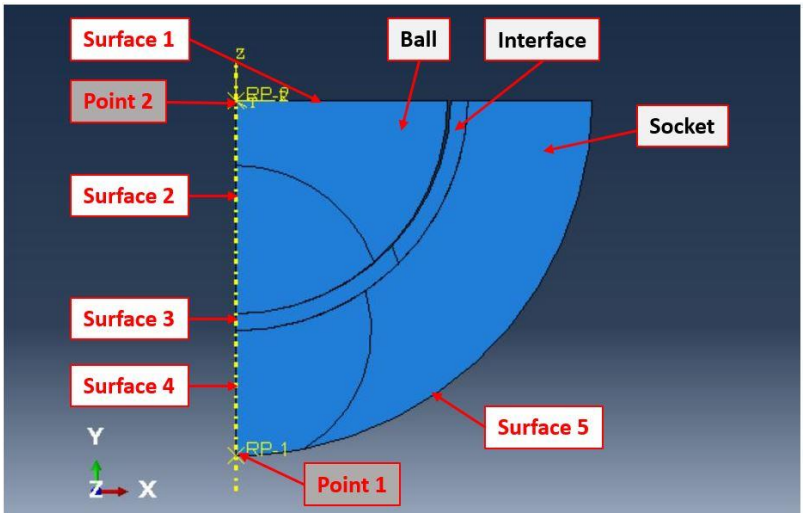

Fig. 14. Boundary conditions for FE model.

The maximum occurring contact pressures and von Mises effective stresses for the different interface materials, as functions of vertical compressive joint loads are presented in Figs. 15 and 16, respectively. The highest von Mises stresses occurred in the interface material. The usual behaviour when pushing two spheres against each other is that the effective stresses are highest a

small distance beneath the surface [27]. The highest effective stresses instead occurred on the interface's upper surface when a large force of 96 kN was applied. It may be a consequence of the excessive clamping and compressive phenomenon in the tight socket combined with the enormous force. The highest stresses occurred beneath the surface when lower loads were used which can be seen by comparing Fig. A1 and A2 in Appendix A, showing von Mises stresses with PEEK-CF30, 5 kN and 96 kN, respectively. FEA contact pressures on a PEEK-CF30 interface material with a load of 5 kN is shown in Fig. 17.

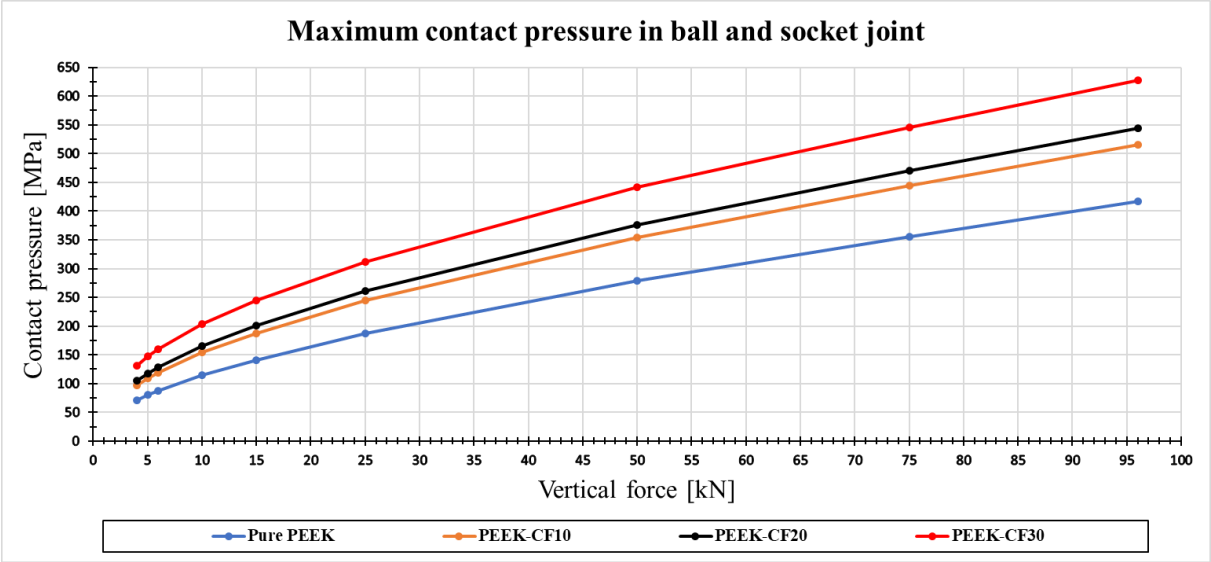

Fig. 15. FE simulated maximum contact pressures in ball joint, from 4 kN to 96 kN.

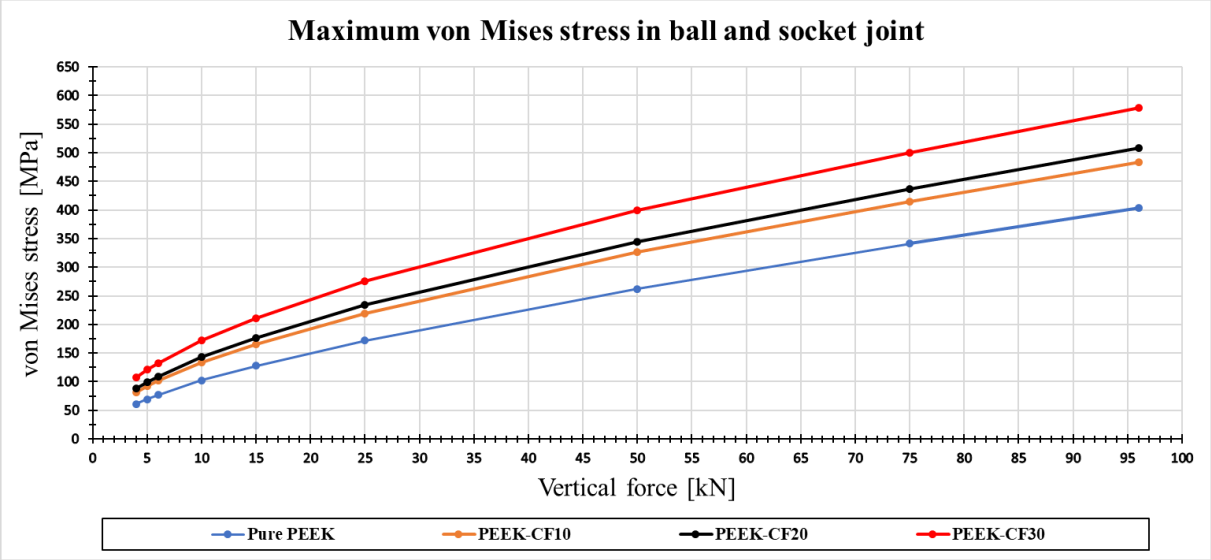

Fig. 16. FE simulated maximum von Mises stresses in ball joint, from 4 kN to 96 kN.

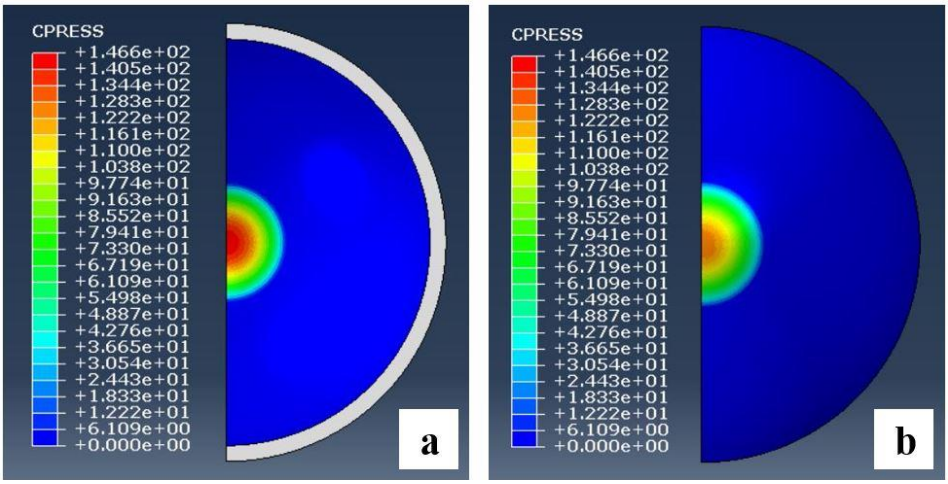

Fig. 17. FEA contact pressures on interface material, PEEK-CF30 with 5 kN load: a) Concave view from above, b) Convex view from beneath.

3.4.2 Hertzian contact mechanics & tribo-discs

The decisions of suitable contact pressures, disc geometries and vertical forces in the tribological tests were an iterative process. There is an impending risk that vertical forces in the SOFS become unstable when too low forces are used. At the other hand, too high forces, contact pressures and stresses increase the risk for catastrophic failure of the tribo-discs which would severely adventure this project's feasibility and outcome. The tribo-discs were finally decided to have a major radius of 25 mm, minor radius of 10 mm and a thickness of 10 mm. The maximum contact pressures in the ball joint obtained from the FE simulations with a 4 kN vertical load were (81, 97, 105 and 131) MPa, for PEEK, PEEK-CF10, PEEK-CF20 and PEEK-CF30, respectively.

According to Hutchings et al. [27], for a spherical point contact with ν=0.3, the maximum shear stress is about 0.31 times the maximum contact pressure and is located beneath the surface at a distance equal to around half of the contact radius. When a horizontal tractional force is present, the maximum tensile stress σ_x in the surface right behind the sliding contact can be described with Eq. 3.1.

$$\sigma_x = p_0\left(\frac{1-2\nu}{3} + \frac{4+\nu}{8}\pi\mu\right) \tag{3.1}$$

p_0 is maximum contact pressure and μ is coefficient of friction [27]. With μ=0.2 and ν=0.4, the latter term in Eq. 3.1 becomes about 0.41. If the two previously mentioned expressions for stresses from vertical and horizontal loads are used as very rough approximations, and with the tensile strength data in Table 2 in mind, the tribo-discs are expected to withstand the contact pressures representing 4 kN in the ball joint.

There exist relatively simple explicit analytical expressions for contact pressures and shear stresses for spherical bodies. For ellipsoids, iterative numerical methods or approximative analytical expressions with correction factors are used. The necessary vertical forces to reach the 4 kN-induced maximum contact pressures were obtained with an internet calculator at www.tribonet.org. The forces are presented in Table 3.

Table 3. Necessary vertical forces in the SOFS for certain contact pressures and disc radii.

Maximum contact pressure [MPa]	Material	Major radius [mm]	Minor radius [mm]	Necessary vertical force [N]
97	PEEK-CF10	25	10	13
105	PEEK-CF20	25	10	11

It is favourable to have the same printing patterns and string directions all over the sliding surfaces. Therefore, the discs were printed with building orientation in the thickness direction and with maximum shell thickness to allow for eventual intense wear. The discs were mounted in a lathe and was manually water-sanded with grit size 1000 silicon carbide paper to remove the rough printing patterns and surface defects. Approximate slicing setup and the polished discs can be seen in Fig. 18.

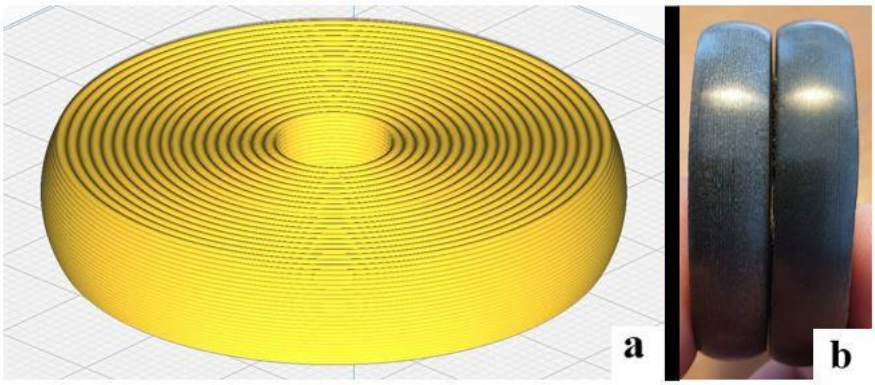

Fig. 18. a) Approximate slicing setup for tribo-disc specimens, b) Polished discs.

3.4.3 Tribological testing

The discs were tested in Karlstad University's SOFS tribotester to analyse friction and wear. In the steam engine, the 3D-printed PEEK-CF will slide against piston rods of austenitic stainless steel. Common approximate surface roughness values for bearing components are in the range of Ra 0.1 – 0.4 µm. In the tribotests, the discs were slid against a 2 mm thick sheet of EN 1.4301 austenitic stainless steel with about 18% Cr and 8% Ni. It had been cold rolled to surface finish 2B, which usually results in Ra values between 0.3 µm and 0.5 µm. EN 1.4301 is also commonly known by the designations AISI 304 or SAE 304.

The SOFS tribotester consists of three rigid beams in a (X, Y, Z) cartesian coordinate system where each beam is connected to an electric stepper motor. The beams are positioned over a large rigid steel table. A disc can be mounted to the Z-beam and slid against a counter material on the table while compressive and tensional strain gauge load cells in the X- and Z-direction collects and stores load data for further friction analyses. Both disc materials were tested in the SOFS with a sliding speed of 0.1 m/s with 390 sliding cycles of 90 mm each resulting in a total sliding distance of approximately 35.1 m. Each sliding test started in a new unworn area and was run in the same line throughout the test with sliding contact occurring in only one direction. The desired vertical forces put into the SOFS software were 13 N and 11 N for PEEK-CF10 and PEEK-CF20, respectively. The two materials were tested in cold water, warm water and in dry conditions. The dry and cold water tests were performed at room temperature. Wooden strips were glued onto the metal sheet with silicone to entrap the water. The temperature in the warm water tests was in the range 50 °C to 80 °C. In the warm water tests, a thermocouple was attached to the metal sheet to obtain real-time temperature information. When the sheet temperature sank below 50 °C, the water was pumped out and replaced with 100 °C boiling water. This cycle took approximately 2.5 min and resulted in the sheet having a temperature between around 50 °C and 80 °C. A thin polymer sheet was placed under the sheet to decrease energy transfer from sheet to table. The tribological SOFS-test matrix can be seen in Table 4 and the SOFS setup is shown in Fig. 19a. Estimations of wear were performed via stereo microscopic analyses.

Table 4. Tribological SOFS-test matrix.

Material	Environment	Vertical force [N]	Sliding speed [m/s]	Sliding distance [m]	Tests per disc
PEEK-CF10	Cold water	13	0.1	35.1	3
PEEK-CF10	Warm water	13	0.1	35.1	2
PEEK-CF10	Dry	13	0.1	35.1	3
PEEK-CF20	Cold water	11	0.1	35.1	3
PEEK-CF20	Warm water	11	0.1	35.1	2
PEEK-CF20	Dry	11	0.1	35.1	3

A MATLAB script was created which read the SOFS data and deleted friction data points in the start and end of each sliding cycle. It was done to decrease the spread of friction data and to only analyse the dynamic coefficient of friction, rather than a combination of static and dynamic COF. The starting values of the COFs obtained in the SOFS tests could not be trusted. Therefore, the COFs for the two materials were tested in cold water and in dry condition in a Forceboard™ friction tester which is displayed in Fig. 19b. The friction curves for cold water and dry condition from the SOFS were calibrated with the starting values obtained with the Forceboard™.

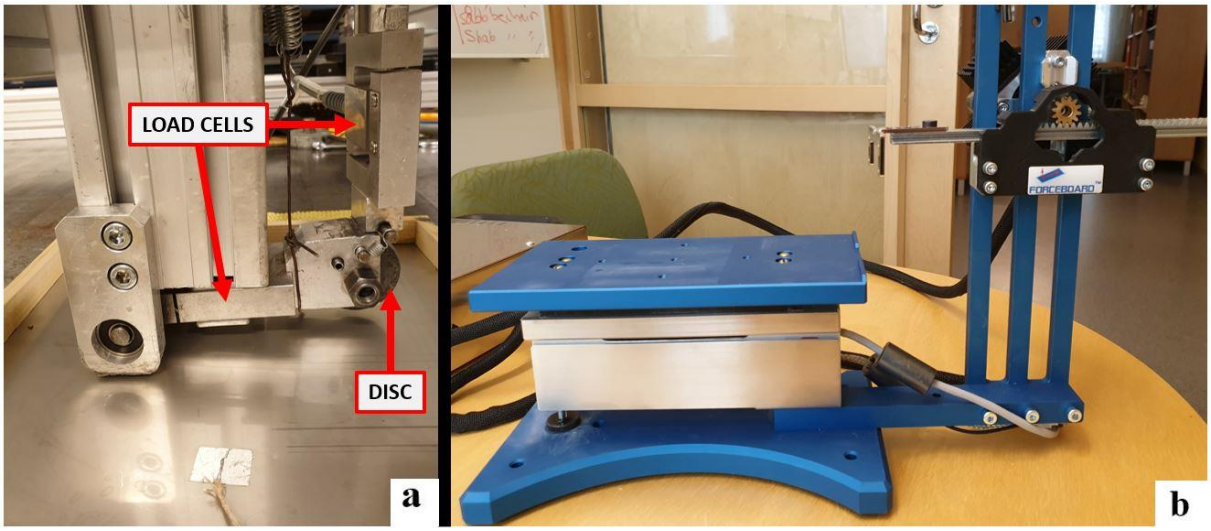

Fig. 19. a) SOFS tribotester, b) Forceboard™ friction tester.

4. Results

4.1 Compressive tests

4.1.1 Strength

Compressive stress-strain curves for horizontal and vertical specimens are shown in Figs. 20 and 21, respectively. A compressive stress-strain graph containing all specimens can be seen in Fig. A4 in Appendix A. Estimations of all specimens' compressive strengths are presented in Fig. 22 where it is seen that the vertical specimens were significantly stronger than the horizontal one's. It can also be concluded that CF20-Horizontal was stronger than CF10-Horizontal while the strength difference between CF20-Vertical and CF10-Vertical was much smaller. Average compressive strength values for the different materials and orientations are presented in Table 5.

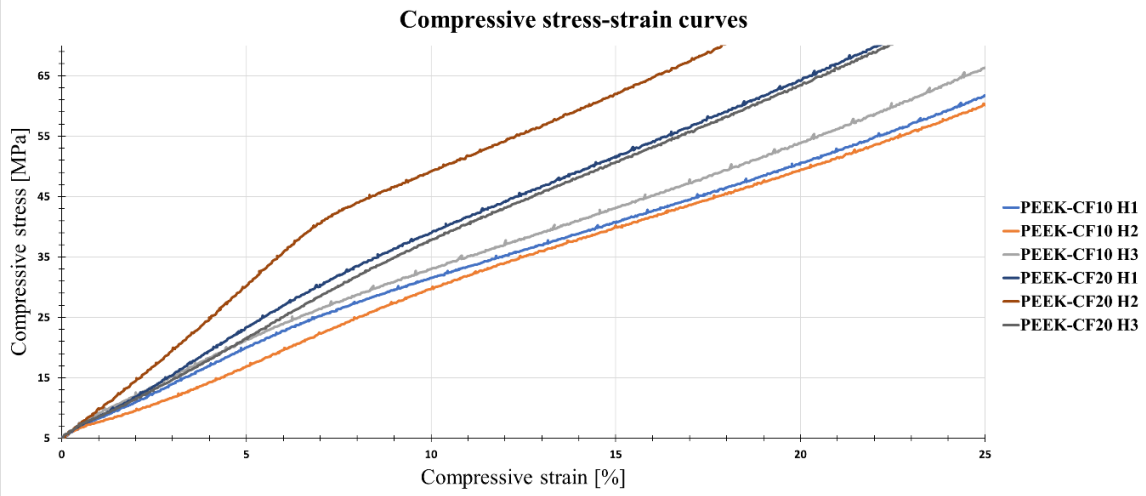

Fig. 20. Compressive stress-strain curves for horizontal specimens.

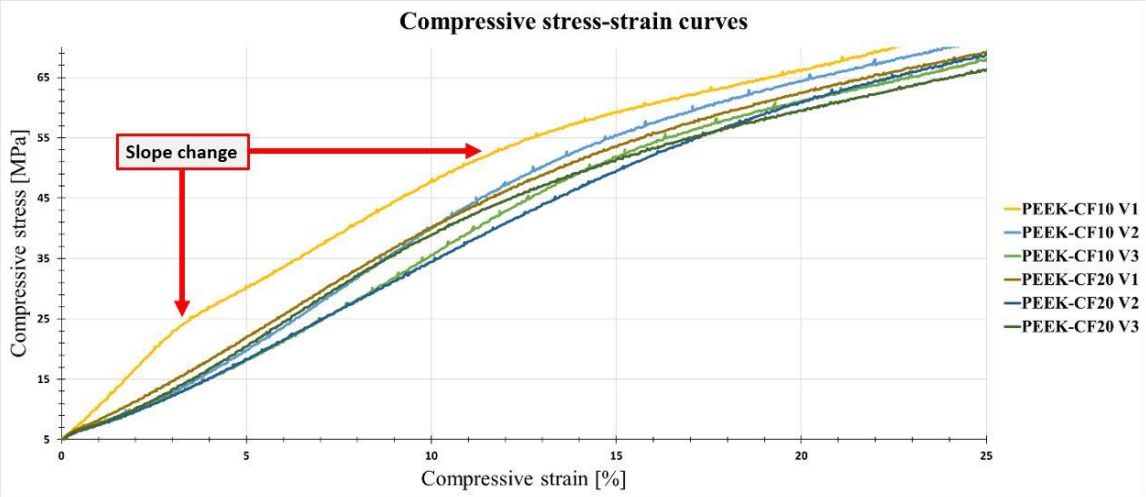

Fig. 21. Compressive stress-strain curves for vertical specimens.

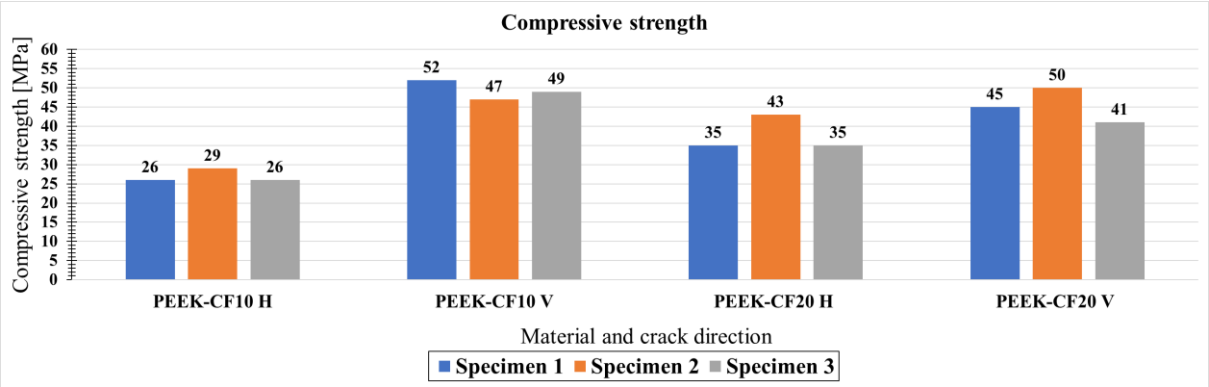

Fig. 22. Diagram with compressive strength results. H=Horizontal, V=Vertical.

Table 5. Average compressive strengths.

Material and orientation	Average compressive strength [MPa]
PEEK-CF10 Horizontal	27
PEEK-CF10 Vertical	49
PEEK-CF20 Horizontal	38
PEEK-CF20 Vertical	45

4.1.2 Stiffness

Estimations of all specimens' compressive stiffnesses were calculated between strains 1% and 3% and are presented in Fig. 23. By inspection of the vertical specimens' compressive stress-strain curves in Fig. 21, it can be noticed that the PEEK-CF10 V1 specimen distinguishes itself by having two pronounced changes of the slope. This indicates that some type of process took place at around 24 MPa, before the yield strength was reached. It is noteworthy that the PEEK-CF10 V1 specimen was the strongest and stiffest of all tested specimens. At strains 1% - 3%, PEEK-CF10 V1 had a stiffness of approximately 0.61 GPa which was more than twice the stiffnesses of CF10 V2 and CF10 V3. After the change of slope, stiffness decreased considerably to about 0.36 GPa.

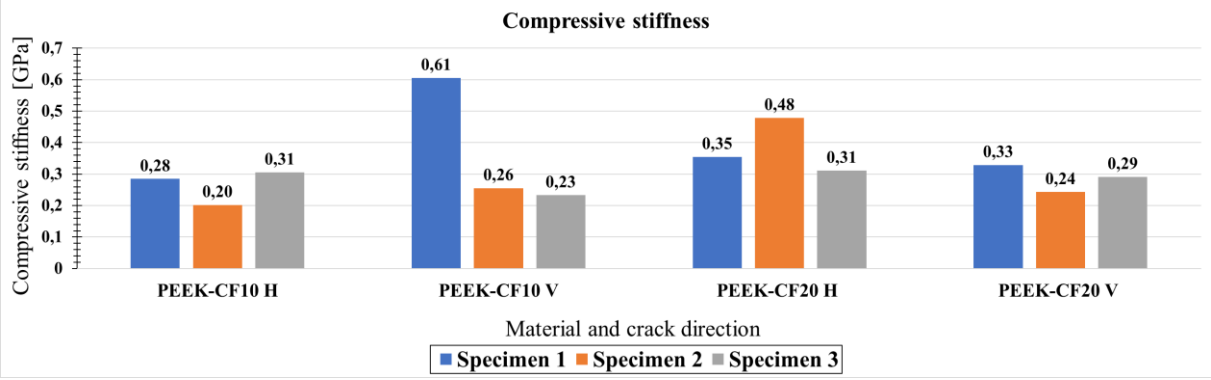

Fig. 23. Diagram with compressive stiffness between 1% and 3% strains. H=Horizontal, V=Vertical.

The very initial parts of the compressive stress-strain curves for horizontal and vertical specimens are shown in Figs. 24 and 25, respectively. An inspection of the initial parts reveals that all other specimens than PEEK-CF10 V1 and PEEK-CF20 H2 seemed to experience stiffness changes at around 5 MPa – 7 MPa. The vertical specimens experienced larger and more distinct slope changes than the horizontal one's. Precise estimations of the specimens' stiffnesses before the first slope changes are difficult to make due to the short linear-like interval. However, the horizontal curves seemed to coincide with PEEK-CF20 H2 while the vertical curves seemed to coincide with PEEK-CF10 V1. Hence, the initial stiffnesses for the horizontal and vertical specimens are roughly estimated to 0.5 GPa and 0.6 GPa, respectively.

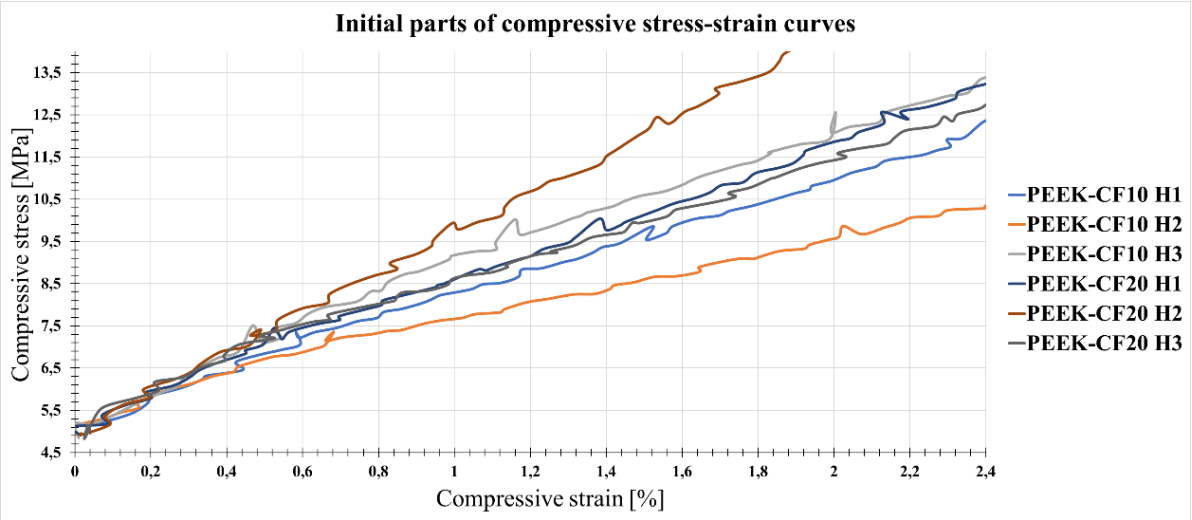

Fig. 24. Initial parts of compressive stress-strain curves for horizontal specimens.

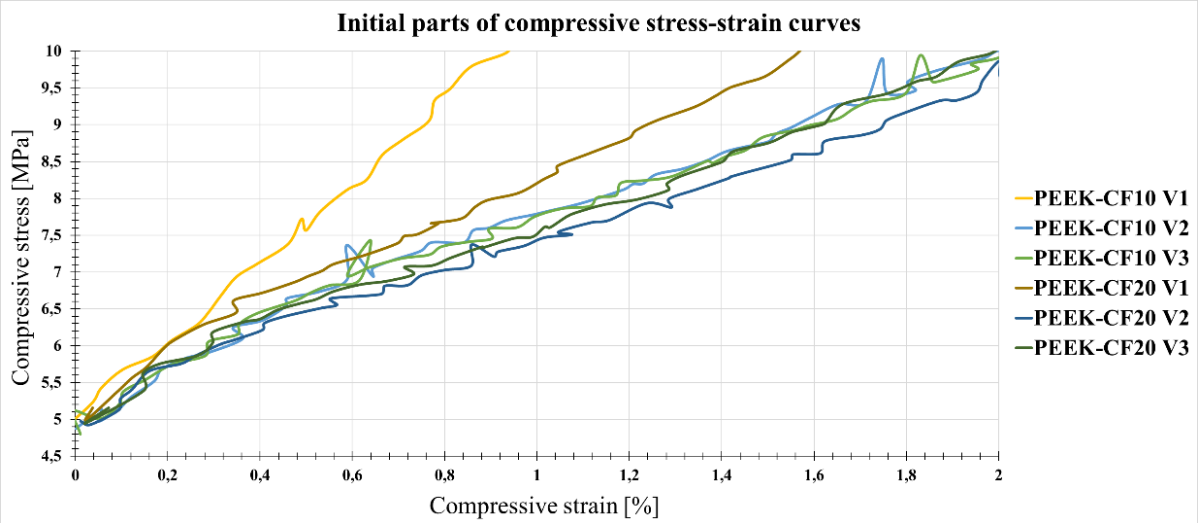

Fig. 25. Initial parts of compressive stress-strain curves for vertical specimens.

Average compressive stiffness values for the different materials and orientations are presented in Table 6. It can be concluded that PEEK-CF20-Horizontal was stiffer than PEEK-CF10-Horizontal. For strains 1% - 3%, the stiffnesses for PEEK-CF10-Vertical were higher than for PEEK-CF20-Vertical. However, the difference was statistically non-existing if the stiffness for PEEK-CF10 V1 between strains 5% - 7% is used.

Table 6. Average stiffness values between 1% and 3% strains, unless otherwise stated.

Material and orientation	Average stiffness values [GPa]
PEEK-CF10 Horizontal	0.26
PEEK-CF10 Vertical	0.36
PEEK-CF10 Vertical, (with CF10 V1 for strains 5% - 7%).	0.28
PEEK-CF20 Horizontal	0.38
PEEK-CF20 Vertical	0.29

4.1.3 Stereo microscopy

Compressed vertical and horizontal specimens were intentionally broken, and their fracture surfaces investigated in a stereo microscope. No significant difference between the different specimen types could be noticed.

The horizontal specimens were equally elongated in the x- and y-direction which is seen in Fig. 26a. In Fig. 26b however, it is clearly seen that the vertical specimens were heavily asymmetrically elongated in the xy-plane. For those specimens, the elongation was largest along the building direction. A sidelong image of a compressed vertical specimen in Fig. 26c exposes a buckling- or bending-like phenomenon of the vertical printing layers.

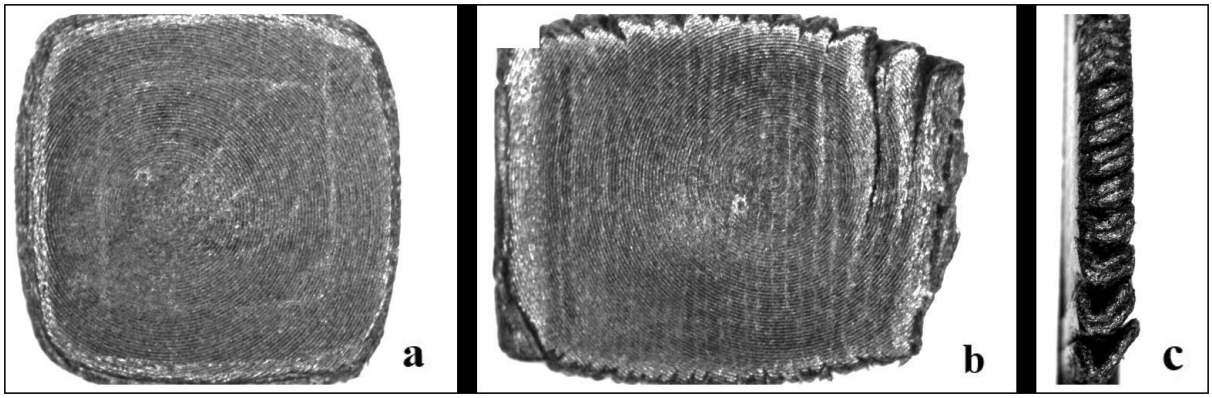

Fig. 26. Stereo microscopy images: a) From above image of compressed horizontal specimen, b) From above image of compressed vertical specimen, c) Sidelong image of compressed vertical specimen.

4.3 Impact strength

Charpy impact strengths with method designation ISO 179-1/1eU, are presented in Fig. 27 for all specimens. The values for the measured impact strengths were relatively gathered in each material and orientation group. Average impact strengths for the different materials and orientations are presented in Table 7 where it can be concluded that the best performing material and crack orientation was PEEK-CF20 and crack arrest, respectively.

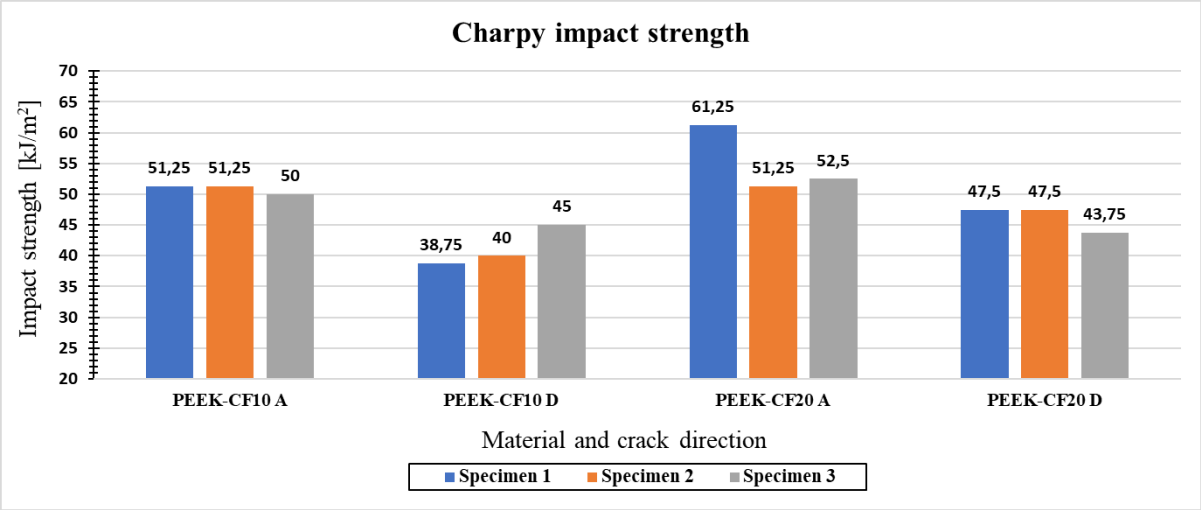

Fig. 27. Diagram with impact strength results. A=Crack arrest, D=Crack divider.

Table 7. Average impact strengths.

Material and crack orientation	Average impact strength [kJ/m^2]
PEEK-CF10 Crack arrest	50.8
PEEK-CF10 Crack divider	41.3
PEEK-CF20 Crack arrest	55.0
PEEK-CF20 Crack divider	46.3

All tested specimens broke into two pieces by brittle fracture. No difference in cracking behaviour was noticed between the PEEK-CF10 and PEEK-CF20 specimens. However, the crack arrest and crack divider specimens fractured in two different ways. The fracture surfaces were relatively flat for crack divider while the fracture surfaces for the crack arrest specimens had a more slant appearance with longer total crack lengths. The noticed differences were relatively consistent in all specimens and typical fractures of crack arrest and crack divider specimens can be seen in Fig. 28-a and b, respectively.

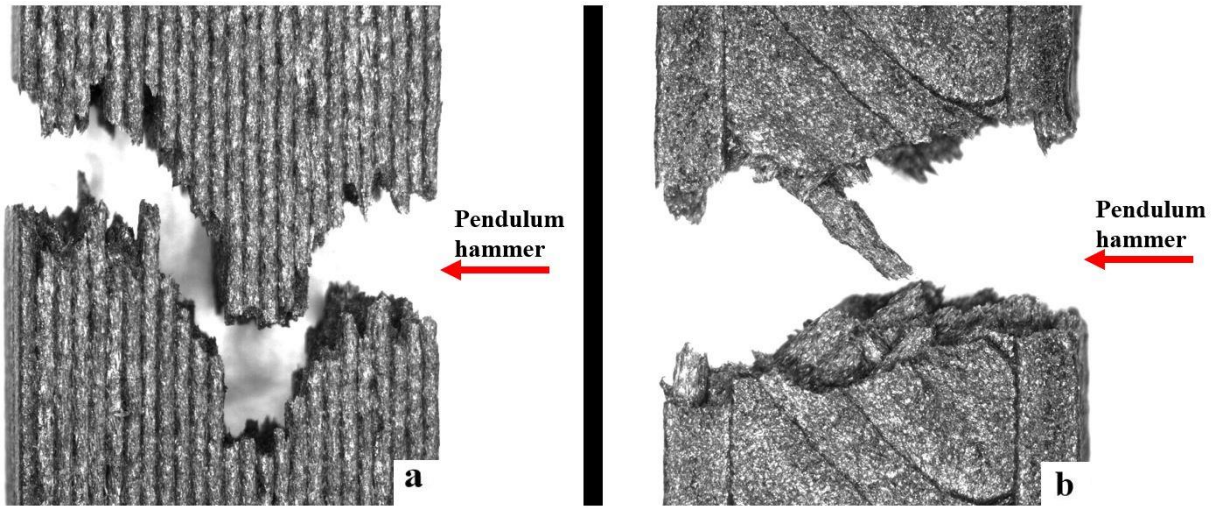

Fig. 28. Typical fractures of impact specimens: a) Crack arrest, b) Crack divider.

4.4 Friction

The obtained friction curves in warm water were alarmingly unstable and are therefore not fully presented in this report. The friction data for warm water had greatly inconsistent starting values and high peaks and low valleys throughout all tests. The horizontal tensional strain gauge load cell in the SOFS tribotester even registered negative and thereby compressive forces for some parts of the warm water-tests, giving the false impression of negative friction. To illustrate the instability in warm water, two curves with COF as function of sliding distance for PEEK-CF10 in warm water are presented in Fig. 29.

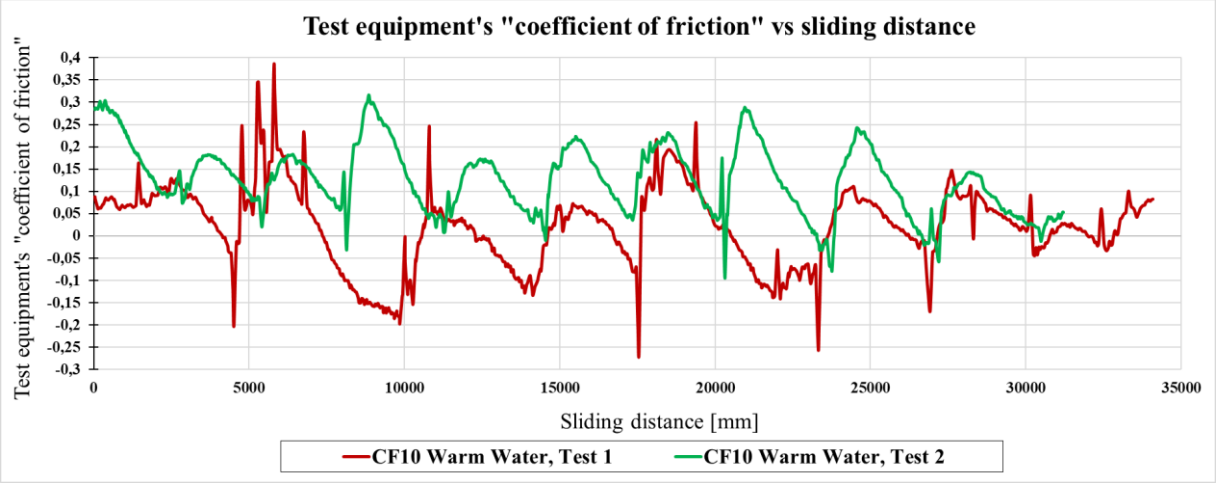

Fig. 29. Test equipment's "coefficient of friction" vs sliding distance for warm water.

The friction curves for cold water and dry condition were much more stable and consistent compared to warm water. Curves with COF as function of sliding distance for PEEK-CF10 and PEEK-CF20 in cold water and dry conditions are presented in Fig. 30. Those curves had been

calibrated with the initial COF values from the Forceboard™ friction tester. By investigating the curves in Fig. 30, it can be concluded that, for the same sliding environment, PEEK-CF10 had higher COF than PEEK-CF20 in both running-in stage and steady-state stage. For the same material, there was higher friction in dry environment than in cold water. During the tested sliding distance, the friction gradually increased in dry environments but gradually decreased in cold water.

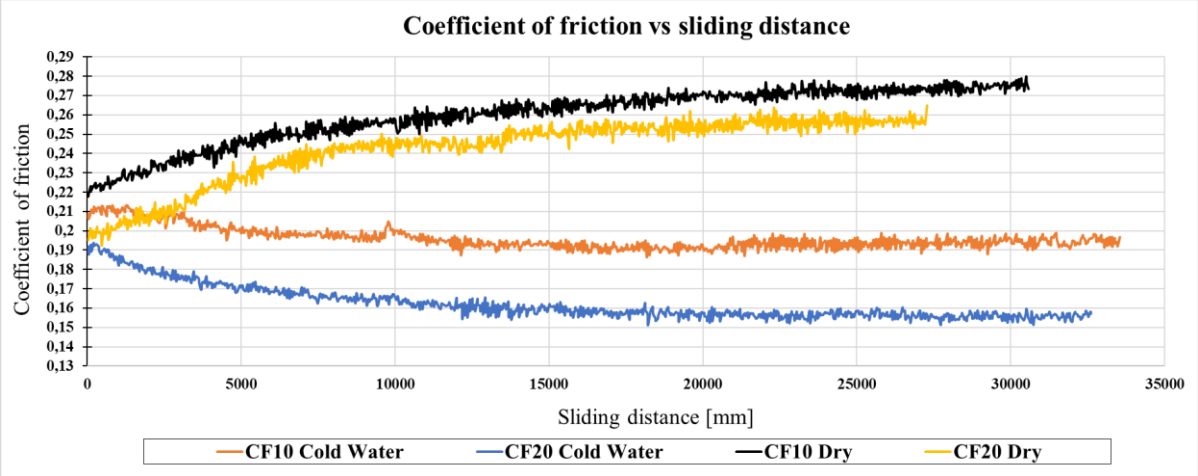

Fig. 30. Coefficient of friction as function of sliding distance.

4.5 Wear

The tribo-disc's wear areas per normal load are presented in Fig. 31 where it can be concluded that warm water caused the most wear and dry environments the least wear. It can also be seen that PEEK-CF20 was more wear-resistant than PEEK-CF10.

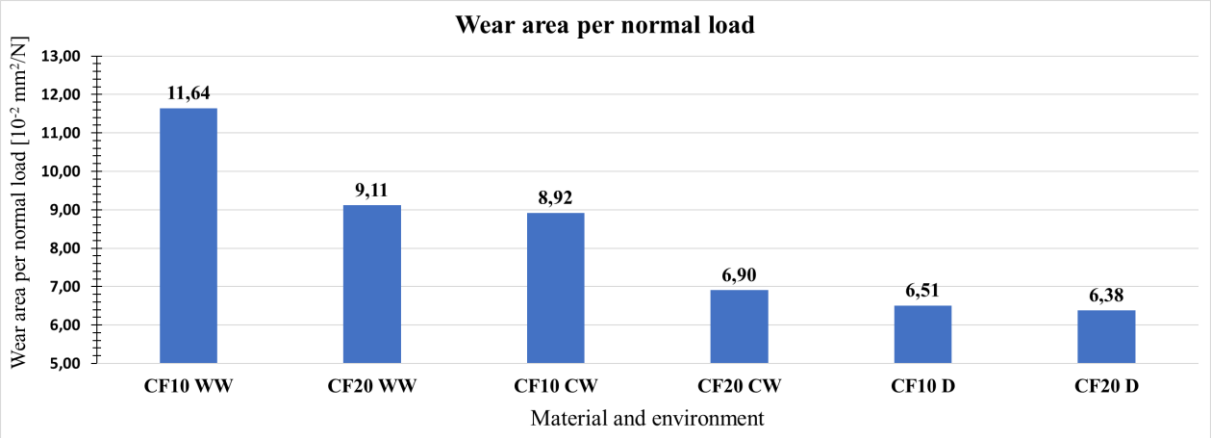

Fig. 31. Diagram with wear area per normal load. WW=Warm water. CW=Cold water. D=Dry.

Representative images of the discs' worn surfaces for each combination of material and sliding environment can be seen in Fig. 32.

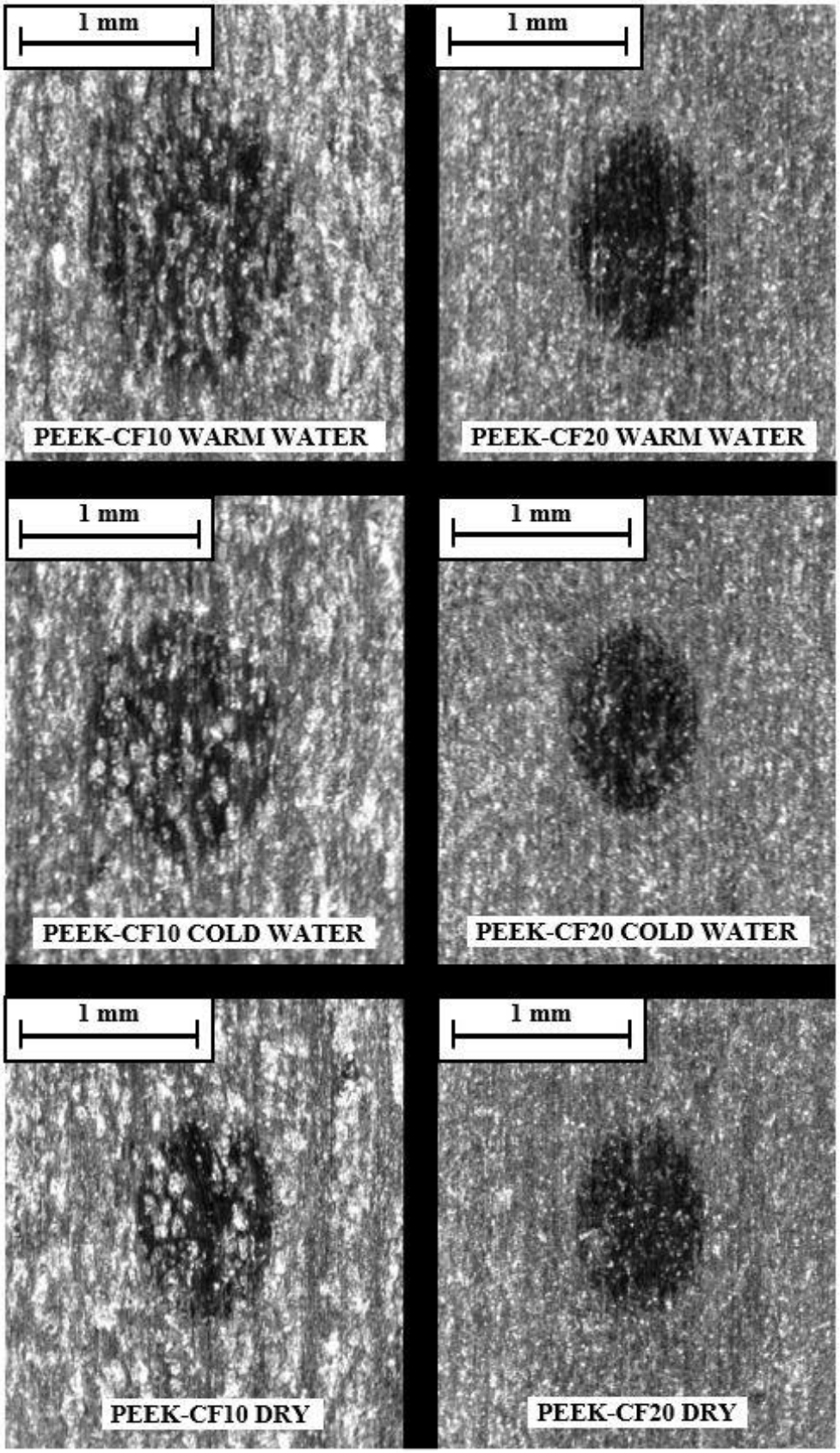

Fig. 32. Representative stereo microscopy images of the discs' worn surfaces. Sliding direction is from top to bottom.

5. Discussion

The maximum force in the steam engine's ball joint, where the PEEK-CF interface material is supposed to be located, is approximately 96 kN. With a ball diameter of 30 mm, a water pressure of around 1400 bar must be present to elevate the ball. The external water pump for the hydrostatic bearings will be able to deliver a water pressure of about 100 bar. However, since water is incompressible, if a check valve is placed between the pump and the ball joint and there is none or very little water leakage out from the joint, a rise of water pressure would be possible when the ball is pushed against the socket. An additional requirement for that to happen is that the stiffness in the socket is sufficiently high, so there is a minimum of volume increase in the socket when the load is applied. Since the piston rod will reciprocate up and down in the engine, albeit not in a pure vertical motion, the forces in the joint will cycle between around 0 and 96 kN. Therefore, a very small water leakage might be possible to tolerate since the socket can be refilled with the 100 bar pressurised water through the check valve when the high pressurised steam is not pushing on the piston head. However, minimizing the water leakage is of crucial importance.

5.1 Compressive tests

The vertical specimens were very anisotropic (see Fig. 26) and are therefore unsuitable in the ball joint since uneven strains in the interface material, which also acts as sealing, can increase the water leakage to unacceptable levels. Uneven deformations can also cause macroscopical peaks and valleys through the ball joint's water film, increasing the probability for contact between piston rod and interface material, leading to higher wear and friction losses. The horizontal specimens' higher degrees of isotropy and equal x- and y-strains, makes them more suitable as bearing- and sealing materials. Rahman's et al. [6] study found that horizontal raster angles of 0°/90° had slightly lower strengths than only 0°. However, it is likely that only 0° would result in unacceptable anisotropy and water leakage, and a compromise may be justified. Even though 0°/90° is more isotropic than only 0°, it is not purely transversally isotropic which would be the best scenario for the application.

In relative terms, the vertical specimens were significantly stronger than the horizontal one's, which probably is due to linearised stress-transferring polymer chains and carbon fibres along the printing direction. Regarding the horizontal specimens, PEEK-CF20-H, (38 MPa) was stronger than PEEK-CF10-H, (27 MPa) and is likely due to more amounts of stress-transferring fibres. Other possible explanations could be better layer- and/or matrix-fibre adhesion that promotes fibre fracture rather than fibre pull-out. Such conclusions would require SEM-analyses, though. The difference in strength between PEEK-CF10-V, (49 MPa) and PEEK-CF20-V, (45 MPa) was insignificant. All tested specimens, horizontal and vertical, had lower strengths (52 MPa as most), than those in

Rahman's et al. [6] study (54 MPa for 0°/90° raster) where exceptionally bad printing parameters were used. Since Han's et al. [32] study with better printing parameters received a compressive strength of 138 MPa, it is reasonable to assume that the printing parameters in this study can be significantly improved. For example, a higher chamber temperature would probably result in better layer- and matrix-fibre adhesion as well as higher degree of crystallinity, which would result in higher strength and stiffness.

Probable explanations to the double slope changes in the compressive stress-strain curves are sliding of printing layers in the horizontal specimens and layer sliding and/or layer buckling in the vertical specimens. It would implicate that the specimens' true compressive stiffnesses were 0.5 GPa and 0.6 GPa for horizontal and vertical specimens, respectively. It was remarkably low values since the filament manufacturers stated the Young's moduli as 8.1 GPa and 10.1 GPa for PEEK-CF10 and PEEK-CF20, respectively, and that the modulus of elasticity for polymers is usually higher in compression than tension [25]. For example, Han's et al. [32] FDM-printed specimens in pure PEEK and PEEK-CF5 exhibited compressive moduli of around 2.8 GPa and 3.5 GPa, respectively. The specimens' low true compressive moduli in this study could have been due to high porosity and/or low crystallinity. But such conclusions would require SEM- and crystallinity analyses. PEEK-CF10-V1's later slope was likely due to higher layer adhesion in that particular specimen. The specimens' stiffnesses after the first slope change were probably a combination of layer friction and the materials' true compressive moduli. Since PEEK-CF20-H2, like PEEK-CF10-V1, was clearly stronger and stiffer than the other specimens, one would with the same reasoning as for PEEK-CF10-V1, expect a later first slope change with PEEK-CF20-H2. However, such an observation was not seen which could have been due to layer sliding occurring after yielding or that the sliding is gradual and difficult to notice. All vertical specimens obtained larger and more distinct first slope changes than the horizontal one's, which is reasonable since the vertical specimens have larger possibilities to layer buckling, bending and deformation in the x- and y-direction. More precise estimations of the true compressive moduli before layer sliding, could likely been obtained if compressive data was logged from 0 MPa instead of 5 MPa.

5.2 Impact tests

Increased strength usually results in decreased impact strength [25]. PEEK-CF20 had higher impact strength than PEEK-CF10 despite higher mean strength. The crack arrest specimens had longer total crack lengths and slant fracture surfaces associated with plane-stress and high toughness. The different behaviours were reflected in the impact results where crack arrest performed better than crack divider. Crack arrest's higher impact strength would motivate a bearing-material in the joint with horizontal printing layers.

5.3 Friction

The most probable explanation to the unsteadiness in the warm-water tests' friction curves is condensed water steam on the load cells' strain gauges which altered their electrical resistance. The load cells reacted clearly and strongly when boiling water was poured onto the metal sheet, even when the SOFS machine was in idle. In its current condition, the SOFS tribotester is therefore unsuitable for friction testing in warm water. Introduction of better sealings of strain gauges or a protective shield under the load cells could improve the SOFS's warm water suitability.

The friction curves had similar behaviours in cold water and in dry condition as in Jacobs' et al [30] study; gradual friction decrease in water and a gradual increase in dry condition. Longer tests and sliding distances had likely resulted in a significant friction decrease for dry sliding after formation of a dense friction-lowering transfer film. However, it is likely that the friction in water had already reached a steady-state stage at $\mu \approx 0.16$.

A deposition tribofilm between a polymer and steel is often immediately destroyed if liquid water is added. It is thought to be due to the so called "hydraulic effect", where water, because of the contact pressure, is squeezed in and out through small pits and pores on the polymer's surface. Despite the transfer film destruction, most polymers sliding against steel exhibit lower friction in water than in dry conditions. The lower friction in water may be explained by water absorption and consequential softening in the polymer's outer sliding surface, which results in lower shear strength and friction. Another possible explanation is that the polymer's lower elastic moduli allow a certain degree of elastohydrodynamic lubrication so that partially asperity-covering water films can be created which lead to a state of mixed lubrication and lower friction [31]. However, an intact water film and mixed lubrication is only possible if the contact pressures are sufficiently low. The lower friction in water in this study may therefore be due to a combination of water absorption and mixed lubrication with a water film.

5.4 Wear

The higher wear in cold water compared to dry conditions could depend on water absorption and/or three-body abrasion of loose rust particles, which was the case in Jacobs' et al. [30] study, described in section 2.6.3. The additional wear increase in warm water could have been due to thermal softening. However, confirmation of these possible explanations would need further analyses. According to Giltrow's et al. [34] criteria, (see section 2.6.3), the tested metal sheet in this study should be susceptible to a dense graphite-transfer film at dry sliding. However, as described in section 2.5.3, tribofilm formations are very dependent on the counter materials' surface roughness, i.e., the metal sheet [29]. In Jacobs' study, the distinct friction decrease occurred first at a sliding

distance of around 80 m. Since no friction-lowering tribofilm seemed to have been formed during this study's tested sliding distance, it is probable that the wear differences between dry and wet conditions would have been larger at longer sliding distances.

5.5 Summary

Considering the specimens' low strengths, a failure of the hydrostatic water pressure would likely lead to immediate breakdown of the PEEK-CF material. Hence, it would be appropriate with a control system that can stop the engine if pressure drop occurs. 3D-printed PEEK-CF is probable relatively cheap to replace if eventual total breakthrough of the water film happens. At partial breakthrough of the water film, it is desirable to maximise strength, impact strength and minimise friction and wear. Stiffness should be maximised to build up water pressure more easily when the ball is pushed down in the socket. The degree of transversal isotropy should be maximised to minimise water leakage through the sealing section. Due to the low degree of transversal isotropy in vertical specimens, PEEK-CF20 with horizontal layers is the most suitable alternative for the application.

6. Future work

The following things are proposals to future work for further understanding and material- and quality improvements:

- Test real prototypes with horizontally printed PEEK-CF20 and estimate endurance, wear and leakage.
- Test other and more combinations of raster angles and investigate its influence of transversal isotropy for horizontally printed parts.
- Perform complete Computation Fluid Dynamics (CFD) and FEM analyses on the ball joint in motion with consideration of viscoelastic effects and polymers' mechanical properties' dependence on hydrostatic pressure. Water film thickness can be optimized and the lowest allowable hydrostatic water pressure can be found.

7. Conclusion

The following conclusions from this project can be drawn:

- Of all tested materials and orientations, horizontally printed PEEK-CF20 had highest stiffness, impact strength and degree of transversal isotropy. PEEK-CF20 exhibited lower friction and wear than PEEK-CF10. Despite that vertically printed PEEK-CF20 was slightly stronger than the horizontally printed, the low degree of transversal isotropy in the vertical specimens may make them unsuitable in the ball joint due to higher risk of water leaks. Hence, horizontally printed PEEK-CF20 is the most suitable material to be used as interfaces and sealings in the steam engine's ball joints.
- Strength and compressive stiffness were low for the tested materials and could most likely be improved with other printing parameters. A higher chamber temperature would probably result in both better layer- and fibre-matrix adhesion as well as higher crystallinity which would lead to higher strength and stiffness.
- Due to the high forces in the ball joint and the interface material's relatively low strength, a total breakthrough of the water film would probably result in immediate failure. Therefore, it would be appropriate with a control system that can stop the engine if pressure drop occurs.
- In the event of unsatisfying performance of the FDM-parts in the prototype tests, it may be considered to print them in printers with higher chamber temperatures or manufacture by injection moulding.

References

[1] Thirunavukkarasu D. Development of inlet valve in an oil-free novel steam engine. [master's thesis on the internet]. Stockholm: Royal Institute of technology; 2021 [cited 2022-03-03]. Available from: https://www.diva-portal.org/smash/record.jsf?pid=diva2%3A1596807&dswid=4462

[2] Löfstrand Grip R. A mechanical model of an axial piston machine. [licentiate thesis on the internet]. Stockholm: Royal Institute of technology; 2009 [cited 2022-03-03]. Available from: http://kth.diva-portal.org/smash/record.jsf?pid=diva2%3A233028&dswid=8218

[3] Kim KH, Kabir E, Ara Jahan S. A review of the consequences of global climate change on human health. Journal of environmental science and health. 2014;32(3):299-318. doi: 10.1080/10590501.2014.941279

[4] Kurtz SM. Synthesis and Processing of PEEK for Surgical Implants. 2nd edition. Oxford: Willam Andrews; 2019

[5] Dua R. Rashad Z. Spears J, Dunn G, Maxwell M. Applications of 3D-Printed PEEK via Fused Filament Fabrication: A Systematic Review. MDPI. 2021;13(4046):162-172. doi: 10.3390/polym13224046

[6] Rahman KM, Letcher T, Reese R. Mechanical properties of additively manufactured peek components using fused filament fabrication. IMECE. 2015:1-11. doi: 10.1115/IMECE2015-52209

[7] Zanjanijam AR, Major I, Lyons JG, Lafont U, Devine DM. Fused Filament Fabrication of PEEK: A Review of Process-Structure-Property Relationships. MDPI. 2020;12(1665):1-29. doi: 10.3390/polym12081665

[8] Qin Q, Li Y, Ma J, Liang Q, Tang B. Mechanical properties and cytotoxicity of hierarchical carbon fiber-reinforced poly (ether-ether-ketone) composites used as implant materials. Journal of the Mechanical Behavior of Biomedical Materials. 2019;89(2):227–233. doi: 10.1016/j.jmbbm.2018.09.040

[9] Granta Edupack.

[10] Baschek G, Hartwig G, Zahradnik F. Effect of water absorption in polymers at low and high temperatures. Polymer. 1999;40:3433–3441. doi: 10.1016/S0032-3861(98)00560-6

[11] Nguyen HX, Ishida H. Poly(Aryl-Ether-Ether-Ketone) and Its Advanced Composites A Review. Polymer composites. 1987;8(2):57–73. doi: 10.1002/pc.750080202

[12] Wang Z, Gao D. Friction and wear properties of stainless steel sliding against polyetheretherketone and carbon-fiber-reinforced polyetheretherketone under natural seawater lubrication. Materials and Design. 2014;53:881–887. doi: 10.1016/j.matdes.2013.07.096

[13] Pai C-C, Jeng R-J, Grossman SJ, Huang J-C. Effects of Moisture on Thermal and Mechanical Properties of Nylon-6,6. Advances in Polymer Technology: Journal of the Polymer Processing Institute. 1989;9(2):157–163. doi: 10.1002/adv.1989.060090206

[14] Lay M, Thajudin NLN, Hamid ZAA, Rusli A, Abdullah MK, Shuib RK. Comparison of physical and mechanical properties of PLA, ABS and nylon 6 fabricated using fused deposition modeling and injection molding. Composites Part B: Engineering. 2019;176(107341). doi: 10.1016/j.compositesb.2019.107341

[15] McGrum NG, Buckley CP, Bucknall CB. Principles of polymer engineering. 2nd edition. New York: Oxford University Press; 1997

[16] Yang C, Tian X, Li D, Cao Y, Zhao F, Shi C. Influence of thermal processing conditions in 3D printing on the crystallinity and mechanical properties of PEEK material. Journal of materials processing technology. 2017;248:1-7. doi: 10.1016/j.jmatprotec.2017.04.027

[17] Chen M, Chung CT. Crystallinity of Isothermally and Nonisothermally Crystallized Poly(Ether Ether Ketone) Composites. Polymer Composites. 1998;19(6):689-697

[18] Rinaldi M, Ghidini T, Gecchini F, Brandao A, Nanni F. Additive layer manufacturing of poly (ether ether ketone) via FDM. Elsevier. 2018;145:162-172

[19] Shanmugam V, Rajendran DJJ, Babu K, Rajendran S, Veerasimman A, Marimuthu U, et al. The mechanical testing and performance analysis of polymer-fibre composites prepared through the additive manufacturing. Elsevier. 2021;93(106925):1-15. doi: 10.1016/j.polymertesting.2020.106925

[20] Manufacturing Guide Sweden AB. Selective Laser Sintering, SLS [internet]. Stockholm: Manufacturing Guide Sweden AB; d.u. [cited 2022-08-25]. Available from: https://www.manufacturingguide.com/en/selective-laser-sintering-sls

[21] Wang P, Zou B, Ding S, Li L, Huang C. Effects of FDM-3D printing parameters on mechanical properties and microstructure of CF/PEEK and GF/PEEK. CSAA. 2021;34(9):236–246. doi: 10.1016/j.cja.2020.05.040

[22] Ding S, Zou B, Wang P, Ding H. Effects of nozzle temperature and building orientation on mechanical properties and microstructure of PEEK and PEI printed by 3D-FDM. Polymer Testing. 2019;78(105948):1-8. doi: 10.1016/j.polymertesting.2019.105948

[23] Wang P, Zou B, Xiao H, Ding S, Huang C. Effects of printing parameters of fused deposition modeling on mechanical properties, surface quality, and microstructure of PEEK. Journal of materials processing technology. 2019;271:62-74. doi: 10.1016/j.jmatprotec.2019.03.016

[24] Spoerk M, Gonzalez-Gutierrez J, Sapkota J, Schuschnigg S, Holzer C. Effect of the printing bed temperature on the adhesion of parts produced by fused filament fabrication. Plastics, Rubber and Composites. 2018;47(1):17-24. doi: 10.1080/14658011.2017.1399531

[25] Hertzberg R, Vinci R, Hertzberg J. Deformation and fracture mechanics of engineering materials. 5th edition. Hoboken: John Wiley & Sons Inc.; 2013

[26] Joyce MR, Starink MJ, Sinclair I. Assessment of mixed mode loading on macroscopic fatigue crack paths in thick section Al-Cu-Li alloy plate. Materials & Design. 2016;93:379–387

[27] Hutchings I, Shipway P. Tribology: Friction and wear of engineering materials. 2nd edition. Oxford: Butterworth-Heinemann; 2017

[28] Fallqvist M. Microstructural, mechanical and tribological characterisation of CVD and PVD coatings for metal cutting applications. Uppsala: Uppsala University; 2012

[29] Jacobson S, Hogmark S. Tribologi-friktion, smörjning, nötning. 2nd edition; 2005

[30] Jacobs O, Jaskulka R, Yan C, Wu W. On the effect of counterface material and aqueous environment on the sliding wear of various PEEK compounds. Tribology Letters. 2005;18(3):359–372. doi: 10.1007/s11249-004-2766-3

[31] Lancaster JK. A review of the influence of environmental humidity and water on friction, lubrication and wear. Tribology international. 1990;23(6):371-389. doi: 10.1016/0301-679X(90)90053-R

[32] Han X, Yang D, Yang C, Spintzyk S, Scheideler L, Li P, et al. Carbon Fiber Reinforced PEEK Composites Based on 3D-Printing Technology for Orthopedic and Dental Applications. Journal of Clinical Medicine. 2019;8(240):1–17. doi: 10.3390/jcm8020240

[33] Li Y, Wang D, Qin W, Jia H, Wu Y, Ma J, et al. Mechanical properties, hemocompatibility, cytotoxicity and systemic toxicity of carbon fibers/poly(ether-etherketone) composites with different fiber lengths as orthopedic implants. Journal of biomaterials science, polymer edition. 2019;30(18):1709–1724. doi: 10.1080/09205063.2019.1659711

[34] Giltrow JP, Lancaster JK. The role of the counterface in the friction and wear of carbon fibre reinforced thermosetting resins. Wear. 1970;16(5):359-374. doi: 10.1016/0043-1648(70)90102-X

Appendix A

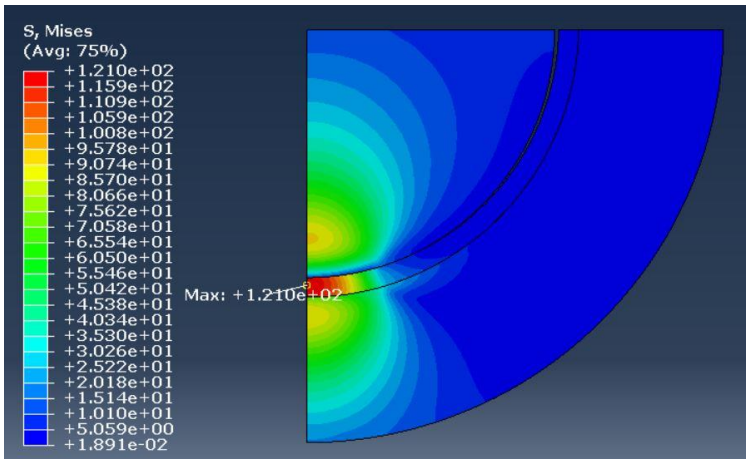

Fig. A1. von Mises stresses in FE simulated ball joint, PEEK-CF30, 5 kN. Maximum stress below interface surface.

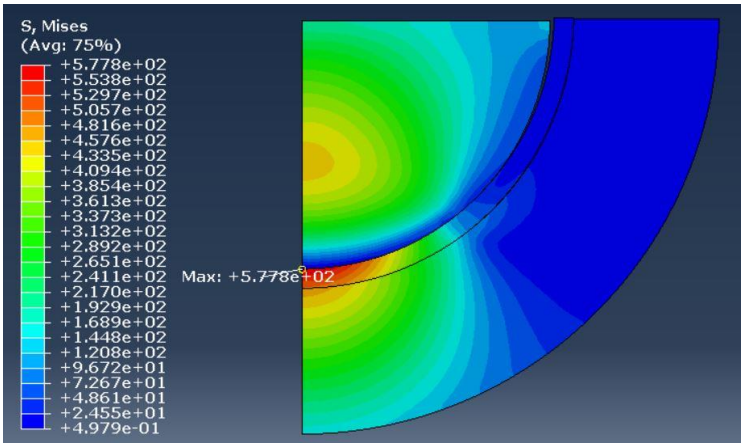

Fig. A2. von Mises stresses in FE simulated ball joint, PEEK-CF30, 96 kN. Maximum stress at upper interface surface.

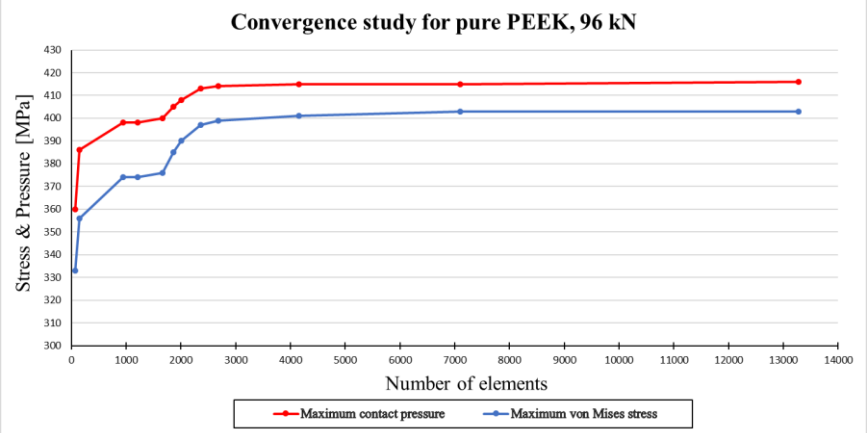

Fig. A3. Convergence study for FEA on ball joint, pure PEEK, 96 kN.

Table A1. The filament suppliers' recommended printing parameters.

Recommended by filament supplier:	**ThermaX PEEK, 3DXTech**	**CarbonX PEEK-CF10, 3DXTech**	**CarbonX PEEK-CF20, 3dXTech**	**Tecafil PEEK-CF30, EnsingerPlastics**
Nozzle temperature [°C]	375 – 410	380 – 410	385 – 415	400 – 440
Chamber temperature [°C]	70 - 140	Recommended	Recommended	230 - 250
Platform temperature [°C]	130 - 145	130 - 150	130 - 150	130 - 160
Annealing [°C]	~~~~	~~~~	~~~~	~~~~
Nozzle diameter [mm]	0.4 mm	Min 0.4 mm	Min 0.4 mm	0.4 - 0.6 mm
Layer height	60% of nozzle diameter	60% of nozzle diameter	60% of nozzle diameter	~~~~
Printing speed:	~~~~	~~~~	~~~~	20 - 30 mm/s

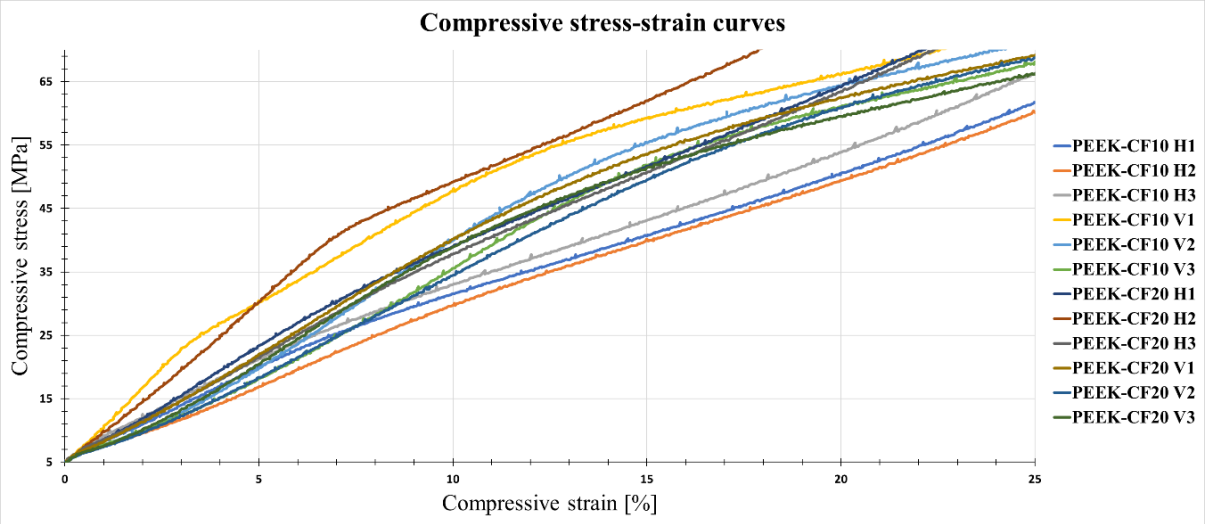

Fig. A4. Compressive stress-strain curves for all specimens. H=Horizontal, V=Vertical.